

Performance Analysis of Integrated Sensing and Communication Networks with Blockage Effects

Ze Zhong Sun, Shi Yan, *Member, IEEE*, Ning Jiang, Jiaen Zhou, and Mugen Peng, *Fellow, IEEE*

Abstract—Communication-sensing integration represents an up-and-coming area of research, enabling wireless networks to simultaneously perform communication and sensing tasks. However, in urban cellular networks, the blockage of buildings results in a complex signal propagation environment, affecting the performance analysis of integrated sensing and communication (ISAC) networks. To overcome this obstacle, this paper constructs a comprehensive framework considering building blockage and employs a distance-correlated blockage model to analyze interference from line of sight (LoS), non-line of sight (NLoS), and target reflection cascading (TRC) links. Using stochastic geometric theory, expressions for signal-to-interference-plus-noise ratio (SINR) and coverage probability for communication and sensing in the presence of blockage are derived, allowing for a comprehensive comparison under the same parameters. The research findings indicate that blockage can positively impact coverage, especially in enhancing communication performance. The analysis also suggests that there exists an optimal base station (BS) density when blockage is of the same order of magnitude as the BS density, maximizing communication or sensing coverage probability.

Index Terms—Integrated sensing and communication (ISAC), performance analysis, blockage effect, stochastic geometry.

I. INTRODUCTION

A. Background and Motivations

INTEGRATED sensing and communication (ISAC) is a potential key technology for beyond-fifth-generation (B5G) and sixth-generation (6G) wireless communications and has received wide attention from academia and industry [1], [2]. ISAC could not only share the same wireless infrastructures to enhance the hardware utilization efficiency but also provide sensing capabilities for wireless networks to obtain information about the surrounding environment [3]–[5]. Dual-function design of communication and radar [6] is a hot issue in ISAC research, which transmits communication information to the receiver and extracts sensing data from the scattered echoes, such as position and velocity. With the development of emerging services such as autonomous driving, industrial

internet of things, and digital twin [7], future dual-functional radar and communication (DFRC) [8] systems are expected to provide sensing applications, e.g., target tracking [9], intrusion detection, and environmental monitoring [10]. In the industry, ISAC is developed in Huawei [11] and ZTE [12] for wireless network investigations. Regarding standardization, 3GPP SA1 has established research project TR 22.837 [13] to discuss the use cases and potential requirements for ISAC while focusing on security and privacy.

The early development of ISAC focused on simultaneously achieving communication and radar functions, with an emphasis on radar sensing [14]. Its evolution went through stages such as coexistence of communication and radar [15], radar-centric communication, and communication-centric radar, gradually evolving into ISAC [16]. In the ISAC systems, the symbiotic relationship between communication and sensing is the linchpin for unlocking their full potential. As these systems evolve from the early stages of exploring communication-radar dynamics to the sophisticated integration of communication and sensing, the need to analyze their performance in real-world scenarios becomes paramount, which is the focus of this paper.

B. Related Works

The research on ISAC performance analysis transitioned from early single-point system performance to network-level system performance. Initial studies concentrated on the ISAC in individual devices or systems, emphasizing how the fusion of these functions could enhance spectrum and energy efficiencies [17], [18], reduce hardware and signal processing costs [19], and explore the performance limits in information theory [20].

The characterization of the trade-off between communication and sensing performance is fundamental to ISAC theory. In [21], the authors derived Cramér-Rao bounds (CRB) for direction, distance, and velocity estimation in single-station uplink scenario, establishing the trade-off relationship between estimation performance and communication rate. Similarly, [22] analyzed the performance of downlink and uplink ISAC systems from an information-theoretic perspective, discussing communication rate (CR), sensing rate (SR), and achievable CR-SR regions in the scenario where a single base station (BS) serves multiple users. In [23], the authors considered a point-to-point model in a dual-function ISAC transmitter scenario, depicting the two-fold trade-offs between achievable communication rates and achievable CRB. Some researchers

Manuscript received XX XXXX 2024; accepted XX XXXX 2024. Date of publication XX XXXX 2024; date of current version XX XXXX 2022. This work was supported in part by XXXX. The associate editor coordinating the review of this article and approving it for publication was XXXX XXXX XX. (Corresponding authors: Mugen Peng; Shi Yan.)

The authors are with the State Key Laboratory of Networking and Switching Technology, Beijing University of Posts and Telecommunications, Beijing 100876, China (e-mail: szz@bupt.edu.cn; yanshi01@bupt.edu.cn; creativejn@bupt.edu.cn; circularje@bupt.edu.cn; pmg@bupt.edu.cn).

Color versions of one or more figures in this article are available at <https://doi.org/10.1109/TVT.2024.0000000>.

Digital Object Identifier 00.0000/TVT.2024.0000000

dedicated efforts to integrated waveform design, where a full-duplex ISAC waveform scheme was devised, and the communication and sensing performances of a half-duplex single-base node were analyzed and optimized [24].

With the continuous advancement of wireless communication and sensing technologies, wireless networks are evolving towards greater density, leading to the extension of ISAC research to the network level [25], [26]. This involves collaborative work among multiple devices, sensors, or nodes to construct more robust and intelligent communication-sensing networks [27]. At the network level, ISAC faces challenges due to the simultaneous communication and sensing tasks of multiple nodes, making the system more susceptible to interference. The rational analysis of inter-BS interference distribution and accurate representation of network performance are crucial for guiding network planning and optimization [28]. Stochastic geometry is commonly employed to model and analyze the spatial layout and location distribution of nodes in wireless networks, providing a powerful analytical framework [29]–[31]. In [32], the authors considered interference constraints in radar-communication networks, deriving the trade-off between radar detection range and network throughput in shared wireless channel scenarios.

However, in practical deployment, especially in urban environments, the previous works often insufficiently consider the blockage effects introduced by buildings. These blockage effects make interference analysis between nodes complex, increasing the difficulty of system performance analysis. In [33], a new mathematical framework was proposed to characterize the coverage probability and ergodic capacity of communication and sensing in ISAC networks. The study analyzed the downlink sensing and communication coverage range and capacity of an ISAC network implemented with OFDM radar. In [34], the spatial distribution of BSs was modeled as a β -Ginibre Point Process (β -GPP), providing insights into the collaborative detection performance of an FD-JCAS system in a heterogeneous millimeter-wave cellular network. In [35], the distribution of blockages in urban areas was modeled by analyzing geographical information system (GIS) measurement statistics, and the successful detection probability and communication probability of ISAC systems were derived. When the impact of blockage was considered in these literatures, the exponential blockage models, generalized LoS sphere models, average probability approaches, and similar methods are always applied to simplify the analysis.

C. Our Contributions

To the best of our knowledge, existing research has rarely considered interference situations simultaneously used for communication and sensing purposes, especially the lack of studies on the performance of ISAC networks in the presence of blockage. In this context, this paper will focus on analyzing the coverage performance of ISAC networks with blockage effects, proposing a general analytical model that is easy to handle. This model avoids mutual interference problems between communication and sensing through the design of time-division duplexing, simultaneously considering several

easy-to-implement special cases, resulting in easy-to-compute closed-form expressions. The main contributions of this paper are summarized as follows:

- Firstly, a generalized framework is proposed through stochastic geometry theory while considering the inherent randomness of BS deployment, signal propagation, target reflection, environmental blockages, and interference. A distance-dependent blockage model is adopted in the urban scenario, which integrates the effects of line of sight (LoS), non-line of sight (NLoS), and target reflection cascading (TRC) paths.
- Secondly, based on the proposed framework, the impact on the ISAC networks coverage performance is evaluated by solving the power loss distribution due to link blockage and the possible interference for each path separately, and expressions for the communication and sensing signal-to-interference-plus-noise ratio (SINR) and the coverage probability are derived.
- Thirdly, special cases such as no blockage and no noise are analyzed. Based on stripping out the influencing factors, closed-form expressions that are easier to compute are derived. It is observed that in some special cases, the communication coverage probability can be independent of the density of BS deployment, but the conditions that make the sensing BS-independent special case will be more demanding.
- Finally, the theoretical accuracy is verified by simulation. The simulation results demonstrate that increasing the BS deployment density can help improve the communication and sensing coverage probabilities within a specific range. The results also show that there exists an optimal BS density that maximizes the communication or sensing coverage probability, and blockage can provide a favorable gain in coverage probability by blocking more interference.

D. Outline of the Paper

The rest of this paper is organized as follows. Section II introduces the general ISAC system model with multiple BSs. Then, Section III evaluates the communication performance and sensing performance, in which the coverage probabilities under various scenarios are derived. Finally, Section IV provides numerical results to verify our analysis before concluding the paper in Section V.

Notations: We use regular, italic, bold lowercase, and bold uppercase letters to denote function names, scalars, vectors, and matrices, respectively. $\mathbb{E}(\cdot)$ denotes the expectation operation. $I_m(\cdot)$ denotes the modified Bessel function of the first kind of order m . $a!$ is the factorial of the nonnegative integer a . $\Gamma(\cdot)$ denotes the gamma function. ${}_2F_1(\cdot)$ denotes the Gauss hypergeometric function. $\text{erfc}(\cdot)$ is the complementary error function. For quick reference, the main mathematical notations used in this paper are summarized in Table I.

II. SYSTEM MODEL

As shown in Fig. 1, we consider an ISAC system with multiple BSs, where there are ISAC BSs, user equipment

TABLE I
 SUMMARY OF NOTATIONS

Notation	Description
Φ_{bs}	Set of locations of all ISAC BSs except b_0 .
λ_{bs}	Density of ISAC BSs.
k_L, k_N, k_R	Gain coefficients of the LoS path, NLoS path and echo path.
$\alpha_L, \alpha_N, \alpha_R$	Path loss exponents of the LoS path, NLoS path and echo path.
$g_{L,i}^{\text{sens}}, g_{N,i}^{\text{sens}}, g_{L,i}^{\text{comm}}, g_{N,i}^{\text{comm}}$	Small-scale fading gain of the LoS and NLoS interference link from the i -th BS to the sensing and communication associated BS.
σ_{rsc}	Radar cross-section of the ST.
b_i	The i -th ISAC BS, where b_0 denotes the sensing and communication associated BS.
$R_i, \tilde{R}_i, \hat{R}_i$	Distance between b_i and UE / ST / b_0 , where R_0 / \tilde{R}_0 denotes the distance between b_0 and UE / ST, and \hat{R}_0 means nothing.
$S_i, \tilde{S}_i, \hat{S}_i$	Independent Bernoulli random variables indicating whether there is a LoS path between b_i and UE / ST / b_0 , where $S_0 = \tilde{S}_0 = 1$, and \hat{S}_0 means nothing.
$\text{PL}_L, \text{PL}_N, \text{PL}_R$	Large-scale path loss functions for LoS, NLoS and echo paths.
Pr_L, Pr_N	Probability of LoS and NLoS propagation.
β	The parameter related to the shape and size of the blockage.
p	The proportion of the area in the region that is blocked.

(UEs), and sensing targets (STs). The locations of BS are modeled as a Poisson point process (PPP) on the \mathbb{R}^2 plane with density of λ_{bs} , denoted as Φ_{bs} . The ISAC BS senses based on echoes. For simplicity, STs are modeled as point targets and are only sensed when a LoS path is present. In contrast, communications will consider both LoS and NLoS paths. On this basis, the typical UE and the typical ST are both associated with the nearest visible BS. For simplicity, it is assumed that the sensing-associated BS and the communication-associated BS are the same and denoted as b_0 .

Wireless resources are temporally divided into communication slots and sensing slots, with each BS synchronized through wired connections to ensure simultaneous execution of communication or sensing tasks within the same time slot. Assuming that each sensing echo returns within the sensing slot, which isolates mutual interference between communication and sensing. Additionally, the slot allocation ratio can be adjusted based on different service requirements to enhance the flexibility of communication sensing functions.

A. Path Loss and Blockage Model

The large-scale path loss functions for LoS and NLoS paths can be expressed as

$$\text{PL}_L(r) = k_L r^{-\alpha_L}, \quad \text{PL}_N(r) = k_N r^{-\alpha_N}, \quad (1)$$

where k_L and k_N are coefficients of the LoS path and NLoS path, and α_L and α_N are the path loss exponents for both. Similarly, the sensed LoS echo path loss can be derived from the monostatic radar equation as

$$\text{PL}_R(r) = k_R r^{-\alpha_R}, \quad (2)$$

where $k_R = k_L/4\pi$ is the gain coefficient of the echo path, and $\alpha_R = 2\alpha_L$ is its road loss exponent.

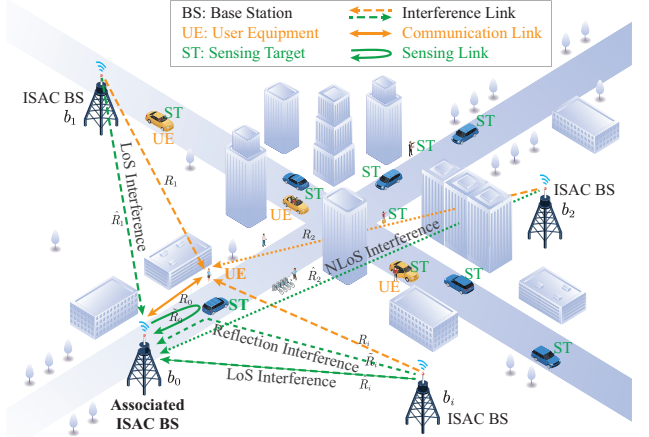


Fig. 1. Schematic diagram of the considered system model.

Assume a Boolean scheme for blockage formation of rectangles. The centers of the rectangles form a homogeneous PPP with density λ_{bk} . The length L_k and the width W_k of the rectangles are assumed to be i.i.d. According to Theorem I in [36], the number of blockages is a Poisson random variable with the mean $\beta R + p$. The probability of being blocked is related to the link length, and the LoS and NLoS probabilities for a link of length R can be modeled as

$$\text{Pr}_L(r) = e^{-(\beta r + p)}, \quad \text{Pr}_N(r) = 1 - \text{Pr}_L(r), \quad (3)$$

where $\beta = 2\lambda_{\text{bk}}(\mathbb{E}[L] + \mathbb{E}[W])/\pi$ is the parameter related to the shape and size of the blockage and $p = \lambda_{\text{bk}}\mathbb{E}[L]\mathbb{E}[W]$ is the proportion of the area in the region that is blocked. Specific typical values can be selected for different scenarios according to the 3GPP TS 38.901 standard [37].

Assuming that the number of blockages on the link is independent, the probability density function (PDF)¹ of the distance R_0 (or \tilde{R}_0) from the UE (or ST) to the nearest visible BS is then [36]

$$f_{R_0}(r) = 2\pi\lambda_{\text{bs}}r e^{-(\beta r + p + 2\pi\lambda_{\text{bs}}U(r))}, \quad (4)$$

where $U(r) = (e^{-p}/\beta^2)[1 - (\beta r + 1)e^{-\beta r}]$. Its integral does not satisfy the normalization condition and can be calculated as

$$\begin{aligned} F_{R_0}(r) &= \int_0^{\infty} f_{R_0}(r) dr \\ &= 1 - \exp\left(-\frac{2e^{-p}\lambda_{\text{bs}}\pi}{\beta^2}\right). \end{aligned} \quad (5)$$

In particular, when both β and p tend to 0,

$$U^o(r) = \lim_{p \rightarrow 0} \lim_{\beta \rightarrow 0} U(r) = \frac{r^2}{2}, \quad (6)$$

the nearest visible association degenerates into the nearest association policy. The PDF of the distance R_0 (or \tilde{R}_0) from the UE (or ST) to the nearest BS is then [38]

$$\begin{aligned} f_{R_0}^o(r) &= \lim_{p \rightarrow 0} \lim_{\beta \rightarrow 0} f_{R_0}(r) \\ &= 2\pi\lambda_{\text{bs}}r e^{-\lambda_{\text{bs}}\pi r^2}. \end{aligned} \quad (7)$$

¹Note: This function does not satisfy the normalization property due to the presence of blockages. Therefore it should not be called a PDF rigorously. However, the probability hypothesis density (PHD) can be used to describe this non-normalized measure.

B. Desired Signal Model

Assuming that the communication-associated BS transmits a constant mode unit signal and that there is a LoS path between the UE and b_0 , the downlink communication received signal is

$$S^{\text{comm}} = g_{L,0}^{\text{comm}} \text{PL}_L(R_0) S_0, \quad (8)$$

where R_0 is the distance from b_0 to UE, and if $S_0 = 1$ then it means that there is a LoS path between b_0 and UE. Besides, $g_{L,0}^{\text{comm}}$ is its small-scale fading gain, which obeys Rician distribution.

The sensing is carried out based on the echo signal, where the transmitted signal arrives at the receiver after round-trip large-scale fading and target reflection attenuation, and the received sensing signal can be modeled as

$$S^{\text{sens}} = \sigma_{\text{rcs}} \text{PL}_R(\tilde{R}_0) \tilde{S}_0, \quad (9)$$

where \tilde{R}_0 is the distance from b_0 to ST, and σ_{rcs} is the ST's radar cross-section (RCS). If $\tilde{S}_0 = 1$, it indicates the existence of a LoS path between b_0 and ST; otherwise, it is a NLoS scenario.

According to the previous assumptions, communication and sensing are conducted when LoS is present, so $S_0 = \tilde{S}_0 = 1$ holds constantly.

C. Interference Model

The interference of the communication considers the downlink interference at the UE, so the UE at the origin is chosen as a typical UE. The interference it suffers is mainly composed of two parts, interference from LoS paths $I_{\text{LoS}}^{\text{comm}}$ and interference from NLoS paths $I_{\text{NLoS}}^{\text{comm}}$, which can be expressed as

$$I^{\text{comm}} = I_{\text{LoS}}^{\text{comm}} + I_{\text{NLoS}}^{\text{comm}}, \quad (10)$$

wherein

$$I_{\text{LoS}}^{\text{comm}} = \sum_{i \in \Phi_{\text{bs}}} g_{L,i}^{\text{comm}} \text{PL}_L(R_i) S_i, \quad (10a)$$

$$I_{\text{NLoS}}^{\text{comm}} = \sum_{i \in \Phi_{\text{bs}}} g_{N,i}^{\text{comm}} \text{PL}_N(R_i) (1 - S_i), \quad (10b)$$

where b_0 is the communication-related BS. $g_{L,i}^{\text{comm}}$ and $g_{N,i}^{\text{comm}}$ are the small-scale fading gains on the LoS and NLoS interference links, respectively. Furthermore, R_i is the distance from b_i to UE, and $S_i \sim \text{Bernoulli}(\text{Pr}_L(R_i))$ are independent Bernoulli random variables indicating whether there is a LoS path between b_i and UE.

Since the sensing results are obtained at the BS, according to Slivnyak's theorem, without loss of generality, the BS located at the origin is chosen as the typical sensing analysis node. The interference generated by other BSs can be composed of three parts. If there is a LoS path between the interfering BS and the typical BS, the interference is denoted as $I_{\text{LoS}}^{\text{sens}}$, otherwise it is expressed as $I_{\text{NLoS}}^{\text{sens}}$. In addition, when there is no collaboration between BSs, the interference $I_{\text{TRC}}^{\text{sens}}$ generated at the sensing BS by the signal transmitted by the interfering BS after reflection from the ST should also be considered. Accordingly, the aggregated sensing interference can be derived as

$$I^{\text{sens}} = I_{\text{LoS}}^{\text{sens}} + I_{\text{NLoS}}^{\text{sens}} + I_{\text{TRC}}^{\text{sens}}, \quad (11)$$

wherein

$$I_{\text{LoS}}^{\text{sens}} = \sum_{i \in \Phi_{\text{bs}}} g_{L,i}^{\text{sens}} \text{PL}_L(\hat{R}_i) \hat{S}_i, \quad (11a)$$

$$I_{\text{NLoS}}^{\text{sens}} = \sum_{i \in \Phi_{\text{bs}}} g_{N,i}^{\text{sens}} \text{PL}_N(\hat{R}_i) (1 - \hat{S}_i), \quad (11b)$$

$$I_{\text{TRC}}^{\text{sens}} = \sum_{i \in \Phi_{\text{bs}}} \sigma_{\text{rcs}} k_R \tilde{R}_i^{-\alpha_L} \tilde{S}_i \times \tilde{R}_0^{-\alpha_L} \tilde{S}_0, \quad (11c)$$

where b_0 is the sensing-associated BS, which is assumed to be the same as the communication-associated BS for convenience. $g_{L,i}^{\text{sens}}$ and $g_{N,i}^{\text{sens}}$ are the small-scale fading gains on the LoS and NLoS interference links respectively. Besides, \hat{R}_i is the distance from the i -th interfering BS b_i to b_0 , \tilde{R}_i is the distance from b_i to ST. Furthermore, $\hat{S}_i \sim \text{Bernoulli}(\text{Pr}_L(\hat{R}_i))$ are independent Bernoulli random variables indicating whether there is a LoS path between b_i and b_0 , and $\tilde{S}_i \sim \text{Bernoulli}(\text{Pr}_L(\tilde{R}_i))$ denote the existence of a LoS path between b_i and ST. Notice that $\tilde{S}_0 = 1$ holds constantly.

D. Small-scale Fading Model

For the LoS interference link, assuming that its small-scale fading obeys a Rician distribution and the corresponding instantaneous signal power obeys a scaled non-central chi-squared distribution with two degrees of freedom, its PDF can be expressed as

$$f_{g_{L,i}^{c/s}}(x) = (1 + K) e^{-K - (1+K)x} I_0 \left(2\sqrt{K(1+K)x} \right), \quad (12)$$

where "c/s" means "comm" or "sens", K is the Rician factor, denoting the ratio of the power in the dominant component to the average power in the diffuse components, $I_0(\cdot)$ denotes the modified Bessel function of the first kind and zero order. The PDF can be approximated by a finite exponential series as [39]

$$f_{g_{L,i}^{c/s}}(x) \approx \sum_{n=0}^N w_n^K u_n^K e^{-u_n^K x} \quad (x \in [0, W]), \quad (13)$$

where N is the number of terms in the exponential series to achieve the desired accuracy, usually a good approximation can be achieved by setting $N = 4$. Both w_n^K and u_n^K are the real coefficients of the n -th term related to the Rician factor K under the $u_n^K > 0$, ($n = 1, 2, \dots, N$) and $\sum_{n=1}^N w_n^K = 1$ constraints, and $[0, W]$ is the range of x . So, the complementary cumulative distribution function (CCDF) of the desired signal power is approximated by [40]

$$\begin{aligned} \bar{F}_{g_{L,i}^{c/s}}(x) &= \int_x^\infty f_{g_{L,i}^{c/s}}(y) dy \\ &\approx \sum_{n=1}^N w_n^K e^{-u_n^K x}. \end{aligned} \quad (14)$$

For the NLoS interference link, assuming that its small-scale fading obeys a Rayleigh distribution, the corresponding instantaneous signal power obeys an exponential distribution, and its PDF and CCDF can be expressed as

$$f_{g_{N,i}^{c/s}}(x) = \mu_N^{c/s} e^{-\mu_N^{c/s} x} \quad (15)$$

and

$$\begin{aligned}\bar{F}_{g_{N,i}^{c/s}}(x) &= \int_x^\infty f_{g_{N,i}^{c/s}}(y)dy \\ &= e^{-\mu_N^{c/s}x}\end{aligned}\quad (16)$$

respectively, where $\mu_N^{c/s}$ is the Rayleigh fading parameter.

For self-receiving and BS₁-sending BS₂-receiving reflection paths, the returned signal power per pulse is assumed to be constant for the time on target during a single scan, but fluctuate independently from scan to scan, following i.i.d. exponential distributions. This corresponds to the Swerling I model commonly used in radar settings [41]. Under this assumption, the PDF for σ_{rcs} in Eqs. (9) and (11c) can be expressed as follows

$$f_{\sigma_{\text{rcs}}}(\sigma) = \frac{1}{\bar{\sigma}_{\text{rcs}}} e^{-\frac{\sigma}{\bar{\sigma}_{\text{rcs}}}}, (\sigma \geq 0), \quad (17)$$

where $\bar{\sigma}_{\text{rcs}}$ is the average of RCS. Its CCDF can be expressed as

$$\bar{F}_{\sigma_{\text{rcs}}}(\sigma) = \int_\sigma^\infty f_{\sigma_{\text{rcs}}}(y)dy = e^{-\frac{\sigma}{\bar{\sigma}_{\text{rcs}}}}, (\sigma \geq 0). \quad (18)$$

E. Performance Metrics

Communication performance is measured using the traditional coverage probability metric, which is defined as the probability that the SINR of the communication $\text{SINR}^{\text{comm}}$ is greater than the threshold T^{comm} . It is related to the detection threshold, the density of BSs, the road loss exponents, and the blockage-related parameters, which can be denoted as

$$\begin{aligned}p_c^{\text{comm}}(T^{\text{comm}}, \lambda_{\text{bs}}, \alpha_L, \alpha_N, \beta, p) \\ = \mathbb{P}[\text{SINR}^{\text{comm}} > T^{\text{comm}}].\end{aligned}\quad (19)$$

The $\text{SINR}^{\text{comm}}$ can be directly expressed as

$$\text{SINR}^{\text{comm}} = \frac{S^{\text{comm}}}{I^{\text{comm}} + N^{\text{comm}}}, \quad (20)$$

where N^{comm} is the additive noise power of communication.

The sensing task is divided into target detection and parameter estimation, with detection performance characterized by the probability of detection and estimation performance described by the accuracy of the parameters. When the false alarm probability is fixed, the detection probability obtained using the Neyman-Pearson detection criterion is directly related to the SINR of sensing $\text{SINR}^{\text{sens}}$ [3].

The probability that $\text{SINR}^{\text{sens}}$ is greater than the signal processing threshold T^{sens} is defined as the sensing coverage probability (or successful detection probability), which can be given by

$$\begin{aligned}p_c^{\text{sens}}(T^{\text{sens}}, \lambda_{\text{bs}}, \alpha_L, \alpha_N, \alpha_R, \beta, p) \\ = \mathbb{P}[\text{SINR}^{\text{sens}} > T^{\text{sens}}].\end{aligned}\quad (21)$$

The sensing SINR is defined as

$$\text{SINR}^{\text{sens}} = \frac{S^{\text{sens}}}{I^{\text{sens}} + N^{\text{sens}}}, \quad (22)$$

where N^{sens} is the additive noise power of sensing.

In the time-division multiplexing system, assuming that the communication and sensing utilize the entire spectrum and power resources in each time slot, allowing for the

evaluation of the snapshot performance of the ISAC network at a specific moment. In this configuration, the proportion of communication to sensing time slots does not directly impact the SINR values for each measurement but may result in a macroscopic loss of achievable communication rates. Its impact on sensing detection probability is reflected in coherent or noncoherent cumulative gains, while its effect on estimation accuracy manifests in the allocation ratio of time-frequency resources and the configuration of frame structures.

III. PERFORMANCE ANALYSIS

A. Communication Coverage Probability

Theorem 1: For specific detection threshold T^{comm} , LoS and NLoS path loss exponents α_L and α_N , and blockage parameters p and β , the communication coverage probability, $p_c^{\text{comm}}(T^{\text{comm}}, \lambda_{\text{bs}}, \alpha_L, \alpha_N, \beta, p)$, can be calculated as (23) at the top of the next page, where

$$\mathbb{F}(\varepsilon, \alpha, p(x), h) = \int_h^\infty \frac{xp(x)}{\varepsilon x^\alpha + 1} dx. \quad (25)$$

Proof: The proof is provided in Appendix A. ■

It is interesting to note that, when $\alpha > 2$, there exists a quasi-closed-form solution to the $\mathbb{F}(\cdot)$ function

$$\begin{aligned}\mathbb{F}(\varepsilon, \alpha, 1, h) &= \int_h^\infty \frac{x}{\varepsilon x^\alpha + 1} dx \\ &= \frac{h^{-(\alpha-2)} {}_2F_1\left(1, \frac{\alpha-2}{\alpha}, 2 - \frac{2}{\alpha}, -\frac{h^{-\alpha}}{\varepsilon}\right)}{\varepsilon(\alpha-2)},\end{aligned}\quad (26)$$

where ${}_2F_1(\cdot)$ is a hypergeometric function which can be calculated using the Gamma functions and finite integral as

$${}_2F_1(a, b; c; t) = \frac{\Gamma(c)}{\Gamma(b)\Gamma(c-b)} \int_0^1 \frac{z^{b-1}(1-z)^{c-b-1}}{(1-tz)^a} dz, \quad (27)$$

where $\Gamma(z) = \int_0^\infty t^{z-1} e^{-t} dt$, and it can be computed by modern computers almost as quickly as the basic function.

More particularly, when $\alpha = 4$, there exists a closed-form solution to the $\mathbb{F}(\cdot)$ function as

$$\begin{aligned}\mathbb{F}(\varepsilon, 4, 1, h) &= \int_h^\infty \frac{x}{\varepsilon x^4 + 1} dx \\ &= \frac{\pi - 2 \arctan(h^2 \sqrt{\varepsilon})}{4\sqrt{\varepsilon}}.\end{aligned}\quad (28)$$

Due to the presence of blockages, the distribution of distances between the accessing BS and the served UE is related to the BS density, so even if noise is not taken into account, the derivative function of Theorem 1 with respect to λ_{bs} is still not constantly 0, and the communication coverage probability varies with the BS density λ_{bs} . However, because of the existence of quasi-closed-form expressions at $\alpha > 2$, the optimal BS deployment density for a given parameter can be computed quite easily.

Next, the special case of no blockage is discussed. When $\beta \rightarrow 0$ and $p \rightarrow 0$, the probabilities of LoS and NLoS propagation become $\text{Pr}_L(x) \rightarrow 1$ and $\text{Pr}_N(x) \rightarrow 0$ respectively, and we have $\mathbb{F}(\varepsilon, \alpha, 0, h) = 0$. The PDF of the distance R_0 from the UE to the nearest BS is then $f_{R_0}(r) \rightarrow f_{R_0}^0(r)$.

$$p_c^{\text{comm}}(T^{\text{comm}}, \lambda_{\text{bs}}, \alpha_L, \alpha_N, \beta, p) = \int_0^\infty \sum_{n=1}^N w_n^K \exp \left[-\frac{u_n^K r^{\alpha_L} T^{\text{comm}} N^{\text{comm}}}{k_L} \right. \\ \left. - 2\pi \lambda_{\text{bs}} \left[\sum_{m=1}^N w_m^K \mathbb{F} \left(\frac{u_m^K}{u_n^K r^{\alpha_L} T^{\text{comm}}}, \alpha_L, \text{Pr}_L(x), r \right) + \mathbb{F} \left(\frac{\mu_N^{\text{comm}} k_L}{u_n^K r^{\alpha_L} T^{\text{comm}} k_N}, \alpha_N, \text{Pr}_N(x), 0 \right) \right] \right] f_{R_0}(r) dr, \quad (23)$$

$$p_c^{\text{sens}}(T^{\text{sens}}, \lambda_{\text{bs}}, \alpha_L, \alpha_N, \alpha_R, \beta, p) = \int_0^\infty \exp \left[-\frac{r^{\alpha_R} T^{\text{sens}} N^{\text{sens}}}{\bar{\sigma}_{\text{rcs}} k_R} - 2\pi \lambda_{\text{bs}} \left[\sum_{n=1}^N w_n^K \mathbb{F} \left(\frac{u_n^K \bar{\sigma}_{\text{rcs}} k_R}{r^{\alpha_R} T^{\text{sens}} k_L}, \alpha_L, \text{Pr}_L(x), r \right) \right. \right. \\ \left. \left. + \mathbb{F} \left(\frac{\mu_N^{\text{sens}} \bar{\sigma}_{\text{rcs}} k_R}{r^{\alpha_R} T^{\text{sens}} k_N}, \alpha_N, \text{Pr}_N(x), 0 \right) + \mathbb{F} \left(\frac{r^{\alpha_L}}{r^{\alpha_R} T^{\text{sens}}}, \alpha_L, \text{Pr}_L(x), r \right) \right] \right] f_{\bar{R}_0}(r) dr, \quad (24)$$

Corollary 1: When blockage is not considered, the communication coverage probability in Theorem 1 degenerates to

$$p_c^{\text{comm}}(T^{\text{comm}}, \lambda_b, \alpha_L, \cdot, 0, 0) \\ = \sum_{n=1}^N w_n^K \int_0^\infty \exp \left[-\frac{u_n^K r^{\alpha_L} T^{\text{comm}} N^{\text{comm}}}{k_L} \right. \\ \left. - 2\pi \lambda_b \left[\sum_{m=1}^N w_m^K \mathbb{F} \left(\frac{u_m^K}{u_n^K r^{\alpha_L} T^{\text{comm}}}, \alpha_L, 1, r \right) \right] \right] f_{R_0}^\circ(r) dr. \quad (29)$$

In the non-blockage scenario, Corollary 1 leads to some exciting conclusions at $\alpha_L > 2$ or even $\alpha_L = 4$, so the main simplifications of the various combinations considered are (1) noisy networks with path loss exponent $\alpha_L = 4$, (2) interference-limited no noise network with path loss exponent $\alpha_L > 2$, and (3) interference-limited no noise network with path loss exponent $\alpha_L = 4$.

Special Case 1: *No blockage, Noise, $\alpha_L = 4$.* Substituting Eq. (28) into Eq. (29) yields the coverage probability of communication in the non-blockage case as

$$p_c^{\text{comm}}(T^{\text{comm}}, \lambda_{\text{bs}}, 4, \cdot, 0, 0) \\ = \int_0^\infty \sum_{n=1}^N w_n^K \exp \left[-\frac{u_n^K r^4 T^{\text{comm}} N^{\text{comm}}}{k_L} - 2\pi \lambda_b r^2 \right. \\ \left. \times \left[\sum_{m=1}^N w_m^K \frac{\pi - 2 \arctan \left(\sqrt{\frac{u_m^K}{u_n^K T^{\text{comm}}}} \right)}{4 \sqrt{\frac{u_m^K}{u_n^K T^{\text{comm}}}}} \right] \right] f_{R_0}^\circ(r) dr \\ \stackrel{(a)}{=} \pi \lambda_b \sum_{n=1}^N w_n^K \int_0^\infty \exp [-\pi \lambda_b (1 + 2\theta_n^K) v - \vartheta_n^K v^2] dv \\ \stackrel{(b)}{=} \frac{1}{2} \pi \lambda_b \sum_{n=1}^N w_n^K \sqrt{\frac{\pi}{\vartheta_n^K}} \exp [(\lambda_b \Psi_n^K)^2] \text{erfc} [\lambda_b \Psi_n^K], \quad (30)$$

where (a) uses the substitution $r^2 \rightarrow v$, and

$$\begin{cases} \theta_n^K = \sum_{m=1}^N w_m^K \frac{\pi - 2 \arctan \left(\sqrt{\frac{u_m^K}{u_n^K T^{\text{comm}}}} \right)}{4 \sqrt{\frac{u_m^K}{u_n^K T^{\text{comm}}}}}, \\ \vartheta_n^K = \frac{u_n^K T^{\text{comm}} N^{\text{comm}}}{k_L}, \\ \Psi_n^K = \frac{\pi(1 + 2\theta_n^K)}{2\sqrt{\vartheta_n^K}}, \end{cases} \quad (31)$$

and (b) is according to

$$\int_0^\infty e^{-x - bx^2} dx = \frac{1}{2} \sqrt{\frac{\pi}{b}} \exp \left[\left(\frac{a}{2\sqrt{b}} \right)^2 \right] \text{erfc} \left[\frac{a}{2\sqrt{b}} \right], \quad (32)$$

wherein $\text{erfc}(x) = \frac{2}{\sqrt{\pi}} \int_x^{+\infty} e^{-t^2} dt$ is the complementary error function.

This expression is effortless to compute, requiring only a simple $\text{erfc}(x)$ value, and can actually be described as a closed-form expression.

Further, some interesting conclusions can be obtained under this model when noise is not taken into account.

Special Case 2: *No blockage, No Noise, $\alpha_L > 2$.* When the blockage is not considered and the noise power $N^{\text{comm}} \rightarrow 0$ or the interference is much larger than the noise, and the path loss exponent α_L is greater than 2, the communication coverage probability is

$$p_{c, \text{noiseless}}^{\text{comm}}(T^{\text{comm}}, \lambda_{\text{bs}}, \alpha_L, \cdot, 0, 0) \\ = \int_0^\infty \sum_{n=1}^N w_n^K \exp \left[-2\pi \lambda_b \right. \\ \left. \times \left[\sum_{m=1}^N w_m^K \mathbb{F} \left(\frac{u_m^K}{u_n^K r^{\alpha_L} T^{\text{comm}}}, \alpha_L, 1, r \right) \right] \right] f_{R_0}^\circ(r) dr \quad (33) \\ \stackrel{(c)}{=} \pi \lambda_b \sum_{n=1}^N w_n^K \int_0^\infty \exp [-\pi \lambda_b v] \exp [-2\pi \lambda_b \xi_n^K v] dv \\ = \sum_{n=1}^N w_n^K \frac{1}{1 + 2\xi_n^K},$$

where (c) uses the substitution $r^2 \rightarrow v$, and

$$\xi_n^K = \sum_{m=1}^N w_m^K \frac{{}_2F_1 \left(1, \frac{\alpha_L - 2}{\alpha_L}, 2 - \frac{2}{\alpha_L}, -\frac{u_n^K T^{\text{comm}}}{u_m^K} \right)}{\frac{u_m^K}{u_n^K T^{\text{comm}}} (\alpha_L - 2)}. \quad (34)$$

In this case, the communication coverage probability is independent of the BS density λ_{bs} . It only relates to the detection threshold T^{comm} and the path loss exponent α_L .

Special Case 3: *No blockage, No Noise, $\alpha_L = 4$.* Combining the first two special cases and substituting $\alpha_L = 4$ make

the closed-form expression as follows

$$\begin{aligned}
 & p_{c,\text{noiseless}}^{\text{comm}}(T^{\text{comm}}, \lambda_{\text{bs}}, 4, \cdot, 0, 0) \\
 &= \int_0^\infty \sum_{n=1}^N w_n^K \exp \left[-2\pi\lambda_b r^2 \right. \\
 & \times \left. \left[\sum_{m=1}^N w_m^K \frac{\pi - 2\arctan\left(\sqrt{\frac{u_m^K}{u_n^K T^{\text{comm}}}}\right)}{4\sqrt{\frac{u_m^K}{u_n^K T^{\text{comm}}}}} \right] \right] f_{R_0}^o(r) dr \quad (35) \\
 &= \pi\lambda_b \sum_{n=1}^N w_n^K \int_0^\infty \exp[-\pi\lambda_b(1+2\theta_n^K)v] dv \\
 &= \sum_{n=1}^N w_n^K \frac{1}{1+2\theta_n^K},
 \end{aligned}$$

where θ_n^K is given by Eq. (31). Similar to conventional communication results, this is a very easy-to-compute closed-form expression that relates only to the detection threshold T^{comm} .

B. Sensing Coverage Probability

Theorem 2: For specific detection threshold T^{sens} , LoS, NLoS and echo path loss exponents α_L , α_N and α_R , and blockage parameters p and β , the sensing coverage probability, $p_c^{\text{sens}}(T^{\text{sens}}, \lambda_{\text{bs}}, \alpha_L, \alpha_N, \alpha_R, \beta, p)$, can be calculated as (24) at the top of the last page.

Proof: The proof is provided in Appendix B. ■

Similarly to the communication coverage probability, the derivative of Theorem 2 with respect to λ_{bs} is not constantly zero. So, under specific parameter configurations, an optimal deployment density of BSs that maximizes the probability of sensing coverage exists here. In particular, there is a quasi-closed-form solution at $\alpha_L > 2$ and a closed-form solution at $\alpha_L = 4$.

Corollary 2: The sensing coverage probability in the non-blockage scenario is given by

$$\begin{aligned}
 & p_c^{\text{sens}}(T^{\text{sens}}, \lambda_b, \alpha_L, \cdot, \alpha_R, 0, 0) \\
 &= \int_0^\infty \exp \left[-\frac{r^{\alpha_R} T^{\text{sens}} N^{\text{sens}}}{\bar{\sigma}_{\text{rcs}} k_R} \right. \\
 & - 2\pi\lambda_b \left[\sum_{n=1}^N w_n^K \mathbb{F} \left(\frac{u_n^K \bar{\sigma}_{\text{rcs}} k_R}{r^{\alpha_L} T^{\text{sens}} k_L}, \alpha_L, 1, r \right) \right. \\
 & \left. \left. + \mathbb{F} \left(\frac{r^{\alpha_L}}{r^{\alpha_R} T^{\text{sens}}}, \alpha_L, 1, r \right) \right] \right] f_{R_0}^o(r) dr. \quad (36)
 \end{aligned}$$

No matter how the configuration parameters are chosen, it is only possible to make a closed-form solution for Corollary 2 if a further simplification is made - disregarding the effect of reflection path interference and the direct and reflective path loss exponents being equal. This is reasonable in some scenarios, such as in collaborative sensing networks, where signals from other BSs that are reflected past the target can be used as useful signals rather than interference.

Special Case 4: *No blockage, Noise, $I_{\text{TRC}}^{\text{sens}} = 0$, $\alpha_L = \alpha_R = 4$.* Substituting Eq. (28) into Eq. (36), and assuming

$\mathbb{F} \left(\frac{r^{\alpha_L}}{r^{\alpha_R} T^{\text{sens}}}, \alpha_L, 1, r \right) = 0$ yields the coverage probability of sensing in this case as

$$\begin{aligned}
 & p_c^{\text{sens}}(T^{\text{sens}}, \lambda_{\text{bs}}, 4, \cdot, 4, 0, 0) \\
 &= \int_0^\infty \exp \left[-\frac{r^4 T^{\text{sens}} N^{\text{sens}}}{\bar{\sigma}_{\text{rcs}} k_R} - 2\pi\lambda_b r^2 \right. \\
 & \times \left. \left[\sum_{n=1}^N w_n^K \frac{\pi - 2\arctan\left(\sqrt{\frac{u_n^K \bar{\sigma}_{\text{rcs}} k_R}{T^{\text{sens}} k_L}}\right)}{4\sqrt{\frac{u_n^K \bar{\sigma}_{\text{rcs}} k_R}{T^{\text{sens}} k_L}}} \right] \right] f_{R_0}^o(r) dr \quad (37) \\
 &\stackrel{(d)}{=} \pi\lambda_b \int_0^\infty \exp[-\pi\lambda_b(1+2\theta)v - \vartheta v^2] dv \\
 &\stackrel{(e)}{=} \frac{1}{2} \pi\lambda_b \sqrt{\frac{\pi}{\vartheta}} \exp\left[(\lambda_b \Psi)^2\right] \text{erfc}[\lambda_b \Psi],
 \end{aligned}$$

where (d) uses the substitution $r^2 \rightarrow v$, (e) uses Eq. (32), and

$$\begin{cases} \theta = \sum_{n=1}^N w_n^K \frac{\pi - 2\arctan\left(\sqrt{\frac{u_n^K \bar{\sigma}_{\text{rcs}} k_R}{T^{\text{sens}} k_L}}\right)}{4\sqrt{\frac{u_n^K \bar{\sigma}_{\text{rcs}} k_R}{T^{\text{sens}} k_L}}}, \\ \vartheta = \frac{T^{\text{sens}} N^{\text{sens}}}{\bar{\sigma}_{\text{rcs}} k_R}, \\ \Psi = \frac{\pi(1+2\theta)}{2\sqrt{\vartheta}}. \end{cases} \quad (38)$$

This expression is similar to the result in Special Case 1 and is even more straightforward to compute. Further, an even simpler expression exists for the calculation of Corollary 2 when the noise is not taken into account.

Special Case 5: *No blockage, No Noise, $I_{\text{TRC}}^{\text{sens}} = 0$, $\alpha_L = \alpha_R > 2$.* When the blockage is not considered and the noise power $N^{\text{sens}} \rightarrow 0$ or the interference is much larger than the noise and the path loss exponent is greater than 2, the sensing coverage probability is

$$\begin{aligned}
 & p_{c,\text{noiseless}}^{\text{sens}}(T^{\text{sens}}, \lambda_{\text{bs}}, \alpha_L, \cdot, \alpha_L, 0, 0) \\
 &= \int_0^\infty \exp \left[-2\pi\lambda_b \right. \\
 & \times \left. \left[\sum_{n=1}^N w_n^K \mathbb{F} \left(\frac{u_n^K \bar{\sigma}_{\text{rcs}} k_R}{r^{\alpha_L} T^{\text{sens}} k_L}, \alpha_L, 1, r \right) \right] \right] f_{R_0}^o(r) dr \quad (39) \\
 &\stackrel{(f)}{=} \pi\lambda_b \int_0^\infty \exp[-\pi\lambda_b(1+2\xi)v] dv \\
 &= \frac{1}{1+2\xi},
 \end{aligned}$$

where (f) uses the substitution $r^2 \rightarrow v$, and

$$\xi = \sum_{n=1}^N w_n^K \frac{{}_2F_1\left(1, \frac{\alpha_L-2}{\alpha_L}, 2 - \frac{2}{\alpha_L}, -\frac{T^{\text{sens}} k_L}{u_n^K \bar{\sigma}_{\text{rcs}} k_R}\right)}{\frac{u_n^K \bar{\sigma}_{\text{rcs}} k_R}{T^{\text{sens}} k_L} (\alpha_L - 2)}. \quad (40)$$

In this case, the sensing coverage probability is independent of the BS density λ_{bs} and is only related to the detection threshold T^{sens} and the path loss exponent α_L .

TABLE II
RICAIN FADING SIMULATION PARAMETERS

Term Index	$K = 1$		$K = 5$		$K = 10$	
	w_n^K	u_n^K	w_n^K	u_n^K	w_n^K	u_n^K
$n = 1$	-0.8993	1.2475	42.243	2.9576	177.75	3.8741
$n = 2$	5.9324	1.4298	-189.99	3.7559	-338.04	4.3761
$n = 3$	-5.4477	1.7436	192.97	4.1436	297.00	5.3985
$n = 4$	1.4145	2.0326	-44.229	4.7715	-135.71	5.9937

Special Case 6: No blockage, No noise, $I_{TRC}^{\text{sens}} = 0$, $\alpha_L = \alpha_R = 4$. Combining special cases 4 and 5 leads to a closed-form solution expressed as

$$\begin{aligned}
 p_c^{\text{sens}}(T^{\text{sens}}, \lambda_{\text{bs}}, 4, \cdot, 4, 0, 0) &= \int_0^\infty \exp \left[-2\pi \lambda_b r^2 \right. \\
 &\times \left. \left[\sum_{n=1}^N w_n^K \frac{\pi - 2 \arctan \left(\sqrt{\frac{u_n^K \bar{\sigma}_{\text{rcs}} k_R}{T^{\text{sens}} k_L}} \right)}{4 \sqrt{\frac{u_n^K \bar{\sigma}_{\text{rcs}} k_R}{T^{\text{sens}} k_L}}} \right] \right] f_{R_0}^o(r) dr \quad (41) \\
 &= \pi \lambda_b \int_0^\infty \exp[-\pi \lambda_b (1 + 2\theta)v] dv \\
 &= \frac{1}{1 + 2\theta},
 \end{aligned}$$

where θ is given by Eq. (38). Similar to conventional communication results, this is a very easy-to-compute closed-form expression that relates only to the detection threshold T^{sens} .

$$\begin{aligned}
 \text{CRLB}_r^{\text{sens}} &= \frac{c_0^2}{32\pi^2 A^2 \Delta f^2 \text{SINR}^{\text{sens}}} \frac{24(2N_s + 1)}{N_c N_s (N_c + 1) (7N_c N_s - 4)} \\
 \text{CRLB}_v^{\text{sens}} &= \frac{c_0^2}{32\pi^2 A^2 T_d^2 f_c^2 \text{SINR}^{\text{sens}}} \frac{24(2N_c + 1)}{N_c N_s (N_s + 1) (7N_c N_s - 4)} \quad (42)
 \end{aligned}$$

IV. SIMULATION RESULTS AND ANALYSIS

In this section, numerical and Monte Carlo simulation results are given to evaluate the performance of communication and sensing. Unless otherwise specified, the generic parameters are set as follows: the area radius is set to be 1 km, the BS density is set to be 10^{-5} m^{-2} , the system bandwidth is set to be 100 MHz, the noise power spectral density is set to be -174 dBm/Hz , the transmit power is set to be 43 dBm, the gain coefficients of LoS, NLoS and echo paths are set to -75 dB , -90 dB , and -86 dB , respectively, and the path loss exponents are set to 2, 3.2, 4, respectively, the Rayleigh fading parameters are set to 1, the average RCS of the ST is set to 20 dBsm (i.e. 100 m^2 in radar settings [42]), the values of the Ricain fading coefficients u_n^K and w_n^K , mainly borrowed from [40], are shown in Table II. The main parameters are listed in Table III.

The main simulation results are given in Figs. 2-5, where the lines indicate the numerical results, and the markers are the same color as the lines, indicating the Monte Carlo simulation results. In addition, solid lines are used to represent the results related to sensing; dotted lines are used to describe the results related to communication; and the size of the parameters represented by black, red, black, green, and purple increases

TABLE III
PARAMETER SETTING OF THE NETWORK

Parameters	Values
Gain coefficient of the LoS path, k_L	-75 dB
Gain coefficient of the NLoS path, k_N	-90 dB
Gain coefficient of the echo path, k_R	-86 dB
Path loss exponent of the LoS path, α_L	2
Path loss exponent of the NLoS path, α_N	3.2
Path loss exponent of the echo path, α_R	4
Rayleigh fading parameters, $\mu_N^{\text{comm}}, \mu_N^{\text{sens}}$	1
Rician fading factor, K	10
Density of ISAC BSs, λ_{bs}	10^{-5} m^{-2}
Transmit signal power, P_t	43 dBm
Noise power spectral density, P_n	-174 dBm/Hz
Total bandwidth of the system, B	100 MHz
Average RCS of the ST, $\bar{\sigma}_{\text{rcs}}$	20 dBsm
Parameter related to the blockage, β	0.008
Parameter related to the blockage, p	0.1
Number of Monte Carlo simulations	10000
The radius of the area	1 km

in order. The Monte Carlo simulation results are very close to the analytical formulations, confirming the correctness of the proposed model and theoretical formulations.

A. Impact analysis of RCS of ST

Fig. 2 depicts the variation of sensing coverage probability with detection threshold for different ST's average RCS, and the purple dashed line in the figure indicates the communication coverage probability under the same parameters. The figure shows that the effect of RCS on the coverage probability is proportional, and every 10 dB increase in RCS will also bring a 10 dB gain in coverage probability. However, since sensing is a two-way attenuation, the coverage probability of sensing will not exceed the coverage probability of communication, no matter how large the RCS is under the same other parameters.

In addition, the coverage probability cannot reach 1, no matter how small the detection threshold is. In traditional models, the integration result should be equal to 1. However, since the blockage modeling is equivalent to the blockage of a portion of the BSs on the original distance function, Eq. (4) does not satisfy the normalization condition, which leads to a coverage hole. From the theoretical formulation, as the detection threshold approaches 0, the coverage probability becomes an integral of the distance function $f_{R_0}(r)$, the result of which can be obtained from Eq. (5).

B. Impact analysis of BS deployment density

Fig. 3 and Fig. 4 show the trend of communication and sensing coverage probabilities with detection threshold for different BS deployment densities. In these figures, two unconventional phenomena can be observed.

Firstly, coverage holes only occur when the BS density is below a certain level, but conversely, when the BS density is high, the coverage probability at a low detection threshold still tends to approach 1. Secondly, the lines on the graph are not strictly arranged from large to small, and there are intersections between the lines, confirming the differential performance of coverage probability at different BS deployment densities.

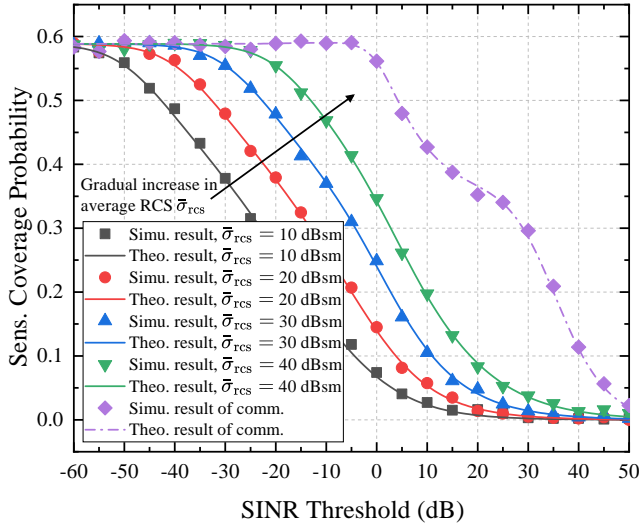


Fig. 2. Variation of sensing coverage probability with detection threshold for different ST's RCS and comparison with that under communication coverage probability with the same parameters.

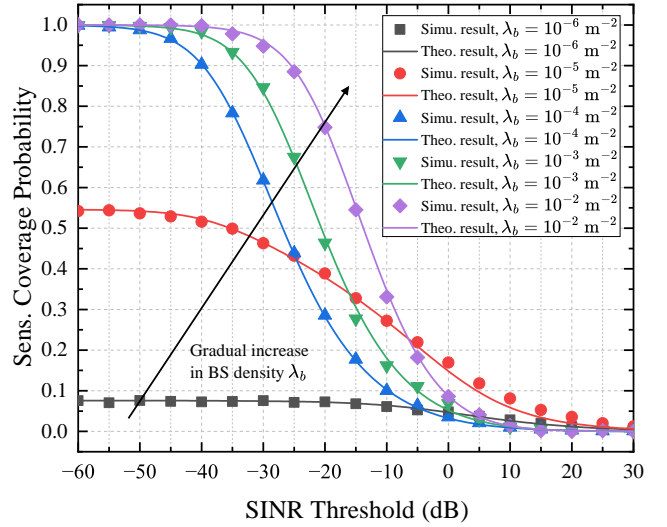


Fig. 4. Variation of sensing coverage probability with detection threshold for different BS deployment densities.

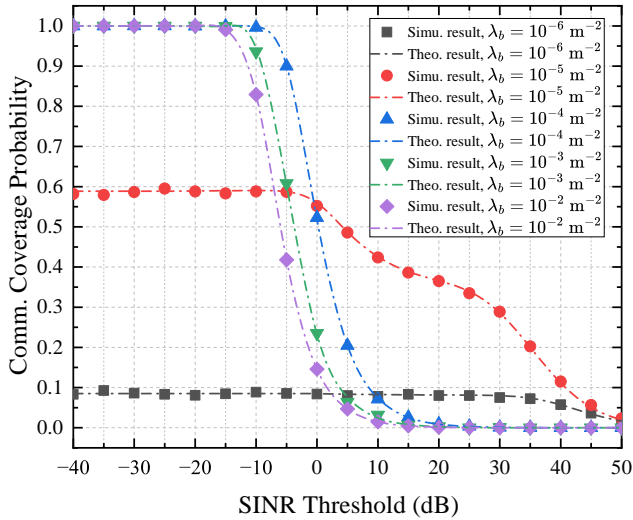


Fig. 3. Variation of communication coverage probability with detection threshold for different BS deployment densities.

To further clarify this variability, Fig. 5 plots the variation of communication and sensing coverage probability with BS deployment density for different detection thresholds. The figure shows that the communication coverage probability exhibits a basic trend of initially increasing and then decreasing with the change in BS density. Due to the access strategy of the nearest visible access, as the BS density increases, the probability of users accessing closer visible BSs increases, leading to an increase in coverage probability. However, on the other hand, increasing the BS density also increases the number of visible interfering BSs. As the gain of useful signals slows down and the attenuation caused by interfering signals gradually becomes dominant, the coverage probability will decrease.

In contrast to the observed communication scenario, sensing coverage probability has two peaks, and the peak points for communication and sensing are not the same. The first peak in sensing occurs near the communication peak. The two peaks in

sensing result from the competition between the useful signal and three interfering components (i.e. interference from LoS, NLoS and TRC links). However, unlike communication, the path loss of the useful signal is a two-way attenuation, so it is more slowly affected by density. Initially, as the BS density increases, the probability of accessing visible BSs increases, leading to an increase in sensing coverage probability. However, since LoS path loss is one-way, the attenuation caused by its interference becomes dominant earlier, resulting in the first peak in sensing, which occurs earlier than the peak in communication. Subsequently, the impact of LoS interference gradually diminishes, and the useful signal again becomes dominant, continuing to increase the coverage probability, resulting in the second peak in sensing coverage probability. Finally, interference from target reflection signals gradually becomes dominant, causing a slight decrease in coverage probability.

Under the current parameter settings, the main peaks of both communication and sensing are concentrated between 10^{-5} and 10^{-4} m^{-2} , which happens to be on the same order of magnitude as the blocking density. Therefore, through reasonable BS deployment and threshold settings, it is possible to simultaneously achieve good sensing coverage while ensuring communication coverage.

C. Impact analysis of environmental blockages

Figs. 6 and 7 compare the variation of sensing and communication coverage probabilities with BS deployment density for blockage and non-blockage cases, respectively. Since closed-form solutions exist for Corollary 1 and Corollary 2 only when $\alpha_L > 2$, the parameters are set to $\alpha_L = 2.4$, $\alpha_R = 4.8$ and the rest of the parameters are kept constant for the simulations. An interesting conclusion is that the blockage effectively improves both sensing and communication coverage. This is because we assume that STs and UEs consistently access the nearest visible BS, so the interfering link must be longer than the link of useful signals. The longer the blocked link, the higher

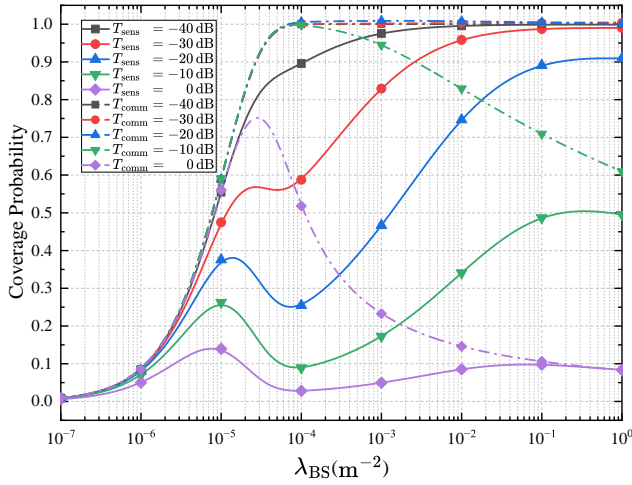


Fig. 5. Variation of coverage probability with BS deployment density for different detection thresholds.

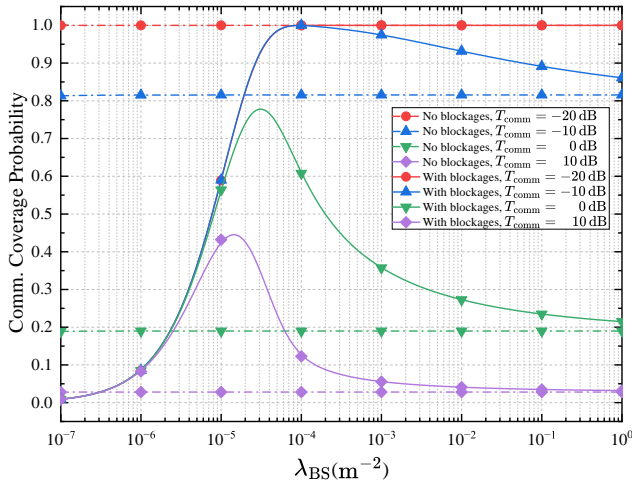


Fig. 6. Variation of communication coverage probability with BS deployment density for blockage and non-blockage scenarios ($\alpha_L = 2.4$, $\alpha_N = 4.8$).

the probability of being blocked, so the presence of blockages makes the interference from the LoS path decrease. As the BS density converges to infinity, both sensing and communication coverage probabilities converge to the non-blockage case, which is the same as the previous conclusion. This is because we also modeled blockage as a PPP independent from the BS, and increasing the BS density to infinity for a fixed blockage density is equivalent to reducing the blockage density to zero. Since the impact of noise on coverage probability is minimal, Fig. 6 already shows that communication coverage probability is independent of BS density in the no blockage case, further confirming the conclusions of theoretical analysis.

V. CONCLUSION

In this paper, we apply a stochastic geometry approach to perform a comprehensive coverage probability performance analysis of ISAC networks, considering the inherent randomness in device deployment, signal propagation, target reflections, environmental blockage, and interference. More specifically, we consider the ISAC networks in the urban

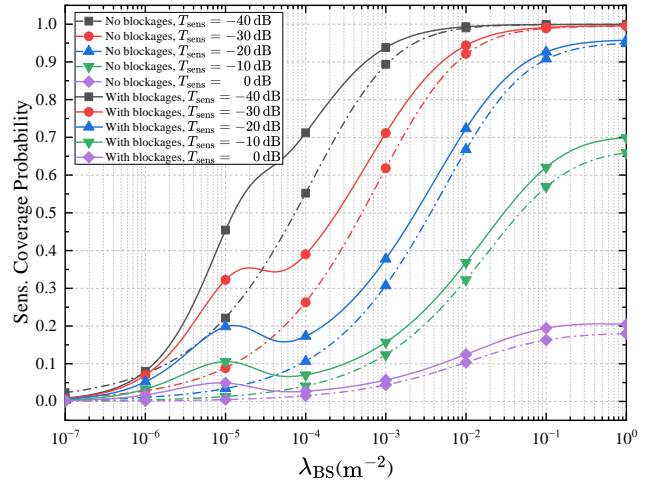


Fig. 7. Variation of sensing coverage probability with BS deployment density for blockage and non-blockage scenarios ($\alpha_L = 2.4$, $\alpha_N = 4.8$).

scenario in the presence of blockages. First, a unified, easy-to-handle system model is developed, which integrates the effects of LoS, NLoS, and target reflected paths. It's also considered the possible blockage effects in ISAC systems and analyzed their impacts on system performance. Then, based on this model, the expressions for the communication and sensing SINR are given separately, and the coverage probability is obtained as a function of BS and blockage densities, detection thresholds, and other system parameters. Last, the special cases of no-blockage noise and no-blockage no-noise are analyzed, the influencing factors are stripped out, and a more easily computable closed-form expression is derived. The simulation results confirm the accuracy of the theoretical results and demonstrate that deploying more BSs is beneficial to improve the communication and sensing coverage probabilities within a certain range. There exists an optimal BS section density and it decreases as the detection threshold increases. On the other hand, the presence of blockages produces a favorable gain in coverage probability. This approach provides valuable insights for designing and optimizing the performance of ISAC systems in real-world scenarios.

APPENDIX A PROOF OF THEOREM 1

In this section, we give the proof of Theorem 1. According to the definition of the coverage probability by the Eq. (19), conditioning on the nearest visible BS being at a distance R_0 from the typical UE, the communication coverage probability can be obtained as

$$\begin{aligned}
 p_c^{\text{comm}}(T^{\text{comm}}, \lambda_{\text{bs}}, \alpha_L, \alpha_N, \beta, p) &= \mathbb{E}_{R_0}[\mathbb{P}[\text{SINR}^{\text{comm}} > T^{\text{comm}} | R_0]] \\
 &= \int_0^\infty \mathbb{P}\left[\frac{g_{L,0}^{\text{comm}} \text{PL}_L(R_0)}{I^{\text{comm}} + N^{\text{comm}}} > T^{\text{comm}} | r\right] f_{R_0}(r) dr \\
 &= \int_0^\infty \mathbb{P}\left[g_{L,0}^{\text{comm}} > \frac{T^{\text{comm}}(I^{\text{comm}} + N^{\text{comm}})}{k_L r^{-\alpha_L}} | r\right] f_{R_0}(r) dr,
 \end{aligned} \tag{43}$$

where $g_{L,0}^{\text{comm}}$ is the small-scale fading gain of the communication desired signal, and substitution into the CCDF approximation of the Rician distribution in Eq. (14) leads to

$$\begin{aligned} & \mathbb{P} \left[g_{L,0}^{\text{comm}} > \frac{T^{\text{comm}} (I^{\text{comm}} + N^{\text{comm}})}{k_L r^{-\alpha_L}} \middle| r \right] \\ & \approx \mathbb{E}_{I^{\text{comm}}} \left[\sum_{n=1}^N w_n^K e^{-\frac{u_n^K r^{\alpha_L} T^{\text{comm}} (I^{\text{comm}} + N^{\text{comm}})}{k_L}} \right] \\ & \stackrel{(a)}{=} \sum_{n=1}^N w_n^K e^{-\frac{u_n^K r^{\alpha_L} T^{\text{comm}} N^{\text{comm}}}{k_L}} \mathcal{L}_{I^{\text{comm}}} \left(\frac{u_n^K r^{\alpha_L} T^{\text{comm}}}{k_L} \right), \end{aligned} \quad (44)$$

where (a) follows from the definition of Laplace transform, and the Laplace function of I^{comm} then can be expressed as

$$\begin{aligned} \mathcal{L}_{I^{\text{comm}}} (s) &= \int_0^\infty e^{-sI^{\text{comm}}} f(I^{\text{comm}}) dI^{\text{comm}} \\ &= \mathbb{E} \left[e^{-sI^{\text{comm}}} \right] \\ &= \mathbb{E} \left[e^{-s(I_{\text{LoS}}^{\text{comm}} + I_{\text{NLoS}}^{\text{comm}})} \right] \\ &= \mathcal{L}_{I_{\text{LoS}}^{\text{comm}}} (s) \mathcal{L}_{I_{\text{NLoS}}^{\text{comm}}} (s). \end{aligned} \quad (45)$$

Since the random variables $g_{L,i}^{\text{comm}}$, S_i , and the point process Φ_{bs} are independent of each other, the order of the expectations and the cumulative multiplication can be exchanged

$$\begin{aligned} & \mathcal{L}_{I_{\text{LoS}}^{\text{comm}}} (s) \\ &= \mathbb{E}_{\Phi_{\text{bs}}, \{g_{L,i}^{\text{comm}}\}, \{S_i\}} \left[e^{-s \sum_{i \in \Phi_{\text{bs}}} g_{L,i}^{\text{comm}} \text{Pr}_L(R_i) S_i} \right] \\ &= \mathbb{E}_{\Phi_{\text{bs}}, \{g_{L,i}^{\text{comm}}\}, \{S_i\}} \left[\prod_{i \in \Phi_{\text{bs}}} e^{-s g_{L,i}^{\text{comm}} k_L R_i^{-\alpha_L} S_i} \right] \\ &= \mathbb{E}_{\Phi_{\text{bs}}} \left[\prod_{i \in \Phi_{\text{bs}}} \mathbb{E}_{\{S_i\}} \left[\mathbb{E}_{\{g_{L,i}^{\text{comm}}\}} \left[e^{-s g_{L,i}^{\text{comm}} k_L R_i^{-\alpha_L} S_i} \right] \right] \right] \quad (46) \\ & \stackrel{(b)}{=} \mathbb{E}_{\Phi_{\text{bs}}} \left[\prod_{i \in \Phi_{\text{bs}}} \mathbb{E}_{\{g_{L,i}^{\text{comm}}\}} \left[e^{-s g_{L,i}^{\text{comm}} k_L R_i^{-\alpha_L}} \right] \right. \\ & \quad \left. \times \text{Pr}_L(R_i) + \text{Pr}_N(R_i) \right], \end{aligned}$$

where (b) uses $S_i \sim \text{Bernoulli}(\text{Pr}_L(R_i))$. Further, the small-scale fading of the LoS path is modeled as Rician fading, whereupon the expectation of the e-exponent with respect to $g_{L,i}^{\text{comm}}$ can be calculated as

$$\begin{aligned} & \mathbb{E}_{\{g_{L,i}^{\text{comm}}\}} \left[e^{-s g_{L,i}^{\text{comm}} k_L R_i^{-\alpha_L}} \right] \\ &= \int_0^\infty e^{-s x k_L R_i^{-\alpha_L}} f_{g_{L,i}^{\text{comm}}} (x) dx \\ & \stackrel{(c)}{\approx} \sum_{n=0}^N w_n^K \int_0^\infty u_n^K e^{-s x k_L R_i^{-\alpha_L}} e^{-u_n^K x} dx \quad (47) \\ &= \sum_{n=1}^N w_n^K \frac{u_n^K}{u_n^K + s k_L R_i^{-\alpha_L}}, \end{aligned}$$

where (c) is obtained using the approximate PDF of $g_{L,i}^{\text{comm}}$ in Eq. (13). Substituting Eq. (47) into Eq. (46) yields that

$$\begin{aligned} & \mathcal{L}_{I_{\text{LoS}}^{\text{comm}}} (s) \\ & \approx \mathbb{E}_{\Phi_{\text{bs}}} \left[\prod_{i \in \Phi_{\text{bs}}} \left[\sum_{n=1}^N w_n^K \frac{u_n^K \text{Pr}_L(R_i)}{u_n^K + s k_L R_i^{-\alpha_L}} + \text{Pr}_N(R_i) \right] \right] \\ & \stackrel{(d)}{=} \exp \left[-2\pi \lambda_{\text{bs}} \int_r^\infty x \left[1 - \sum_{n=1}^N w_n^K \frac{u_n^K \text{Pr}_L(x)}{u_n^K + s k_L x^{-\alpha_L}} \right. \right. \\ & \quad \left. \left. - \text{Pr}_N(x) \right] dx \right] \\ &= \exp \left[-2\pi \lambda_{\text{bs}} \sum_{n=1}^N w_n^K \int_r^\infty x \left(\frac{s k_L \text{Pr}_L(x)}{u_n^K x^{\alpha_L} + s k_L} \right) dx \right] \\ &= \exp \left[-2\pi \lambda_{\text{bs}} \sum_{n=1}^N w_n^K \mathbb{F} \left(\frac{u_n^K}{s k_L}, \alpha_L, \text{Pr}_L(x), r \right) \right], \end{aligned} \quad (48)$$

where (d) uses the probability generation functional [38] (PGFL) of PPP, which states for some function $f(x)$ that

$$\mathbb{E}_{\Phi_{\text{bs}}} \left[\prod_{i \in \Phi_{\text{bs}}} f(x) \right] = \exp \left[- \int_{\mathbb{R}^2} (1 - f(x)) \lambda_{\text{bs}} (dx) \right]. \quad (49)$$

Since the associated BS is the nearest visible BS and there will be no other visible BSs closer than the associated BS, the integral starts at r when using PGFL. The last step in the derivation defines a new function $\mathbb{F}(\cdot)$ which can be expressed as

$$\mathbb{F}(\varepsilon, \alpha, p(x), h) = \int_h^\infty \frac{x p(x)}{\varepsilon x^\alpha + 1} dx. \quad (50)$$

Similarly, for the Laplace transform of the NLoS interference, since the random variables $g_{N,i}^{\text{comm}}$, S_i , and the point process Φ_{bs} are independent of each other, we have

$$\begin{aligned} & \mathcal{L}_{I_{\text{NLoS}}^{\text{comm}}} (s) \\ &= \mathbb{E}_{\Phi_{\text{bs}}, \{g_{N,i}^{\text{comm}}\}, \{S_i\}} \left[e^{-s \sum_{i \in \Phi_{\text{bs}}} g_{N,i}^{\text{comm}} \text{Pr}_N(R_i) (1-S_i)} \right] \\ &= \mathbb{E}_{\Phi_{\text{bs}}, \{g_{N,i}^{\text{comm}}\}, \{S_i\}} \left[\prod_{i \in \Phi_{\text{bs}}} e^{-s g_{N,i}^{\text{comm}} k_N R_i^{-\alpha_N} (1-S_i)} \right] \\ &= \mathbb{E}_{\Phi_{\text{bs}}} \left[\prod_{i \in \Phi_{\text{bs}}} \mathbb{E}_{\{S_i\}} \left[\mathbb{E}_{\{g_{N,i}^{\text{comm}}\}} \left[e^{-s g_{N,i}^{\text{comm}} k_N R_i^{-\alpha_N} (1-S_i)} \right] \right] \right] \\ & \stackrel{(e)}{=} \mathbb{E}_{\Phi_{\text{bs}}} \left[\prod_{i \in \Phi_{\text{bs}}} \left[\mathbb{E}_{\{g_{N,i}^{\text{comm}}\}} \left[e^{-s g_{N,i}^{\text{comm}} k_N R_i^{-\alpha_N}} \right] \right. \right. \\ & \quad \left. \left. \times \text{Pr}_N(R_i) + \text{Pr}_L(R_i) \right] \right], \end{aligned} \quad (51)$$

where (e) uses $S_i \sim \text{Bernoulli}(\text{Pr}_L(R_i))$. The small-scale fading of the NLoS path is modeled as Rayleigh fading, after that the expectation with respect to $g_{N,i}^{\text{comm}}$ can be formulated

as follows

$$\begin{aligned}
 \mathbb{E}\{g_{N,i}^{\text{comm}}\} & \left[e^{-sg_{N,i}^{\text{comm}}k_N R_i^{-\alpha_N}} \right] \\
 & = \int_0^\infty e^{-sxk_N R_i^{-\alpha_N}} f_{g_{N,i}^{\text{comm}}}(x) dx \\
 & \stackrel{(f)}{=} \mu_N^{\text{comm}} \int_0^\infty e^{-x(\mu_N^{\text{comm}} + sk_N R_i^{-\alpha_N})} dx \\
 & = \frac{\mu_N^{\text{comm}}}{\mu_N^{\text{comm}} + sk_N R_i^{-\alpha_N}},
 \end{aligned} \tag{52}$$

where (f) holds because Eq. (15) and μ_N^{comm} is the Rayleigh fading parameters for the communication NLoS interference path. Hence,

$$\begin{aligned}
 \mathcal{L}_{I_{\text{NLoS}}^{\text{comm}}}(s) & \\
 & = \mathbb{E}_{\Phi_{\text{bs}}} \left[\prod_{i \in \Phi_{\text{bs}}} \left[\frac{\mu_N^{\text{comm}} \text{Pr}_N(R_i)}{\mu_N^{\text{comm}} + sk_N R_i^{-\alpha_N}} + \text{Pr}_L(R_i) \right] \right] \\
 & \stackrel{(g)}{=} \exp \left[-2\pi \lambda_{\text{bs}} \int_0^\infty x \left(\frac{sk_N \text{Pr}_N(x)}{\mu_N^{\text{comm}} x^{\alpha_N} + sk_N} \right) dx \right] \\
 & = \exp \left[-2\pi \lambda_{\text{bs}} \mathbb{F} \left(\frac{\mu_N^{\text{comm}}}{sk_N}, \alpha_N, \text{Pr}_N(x), 0 \right) \right],
 \end{aligned} \tag{53}$$

where (g) uses the PGFL, but the integration starts from 0 because there may be other BSs without direct paths within a circle of radius r under the nearest visible access policy.

Multiply the results of (48) and (53), then substitute them into (44) and then into (43) yields the proof. ■

APPENDIX B PROOF OF THEOREM 2

In this section, we give the proof of Theorem 2. According to the definition of the coverage probability by the Eq. (21), conditioning on the nearest visible BS being at a distance \tilde{R}_0 from the typical ST, the sensing coverage probability can be calculated as

$$\begin{aligned}
 p_c^{\text{sens}}(T^{\text{sens}}, \lambda_{\text{bs}}, \alpha_L, \alpha_N, \alpha_R, \beta, p) & \\
 & = \mathbb{E}_{\tilde{R}_0} [\mathbb{P}[\text{SINR}^{\text{sens}} > T^{\text{sens}} | \tilde{R}_0]] \\
 & = \int_0^\infty \mathbb{P}[\text{SINR}^{\text{sens}} > T^{\text{sens}}] f_{\tilde{R}_0}(r) dr \\
 & = \int_0^\infty \mathbb{P} \left[\frac{\sigma_{\text{rcs}} \text{PL}_R(\tilde{R}_0)}{I^{\text{sens}} + N^{\text{sens}}} > T^{\text{sens}} | r \right] f_{\tilde{R}_0}(r) dr \\
 & = \int_0^\infty \mathbb{P} \left[\sigma_{\text{rcs}} > \frac{T^{\text{sens}} (I^{\text{sens}} + N^{\text{sens}})}{k_R r^{-\alpha_R}} | r \right] f_{\tilde{R}_0}(r) dr \\
 & \stackrel{(a)}{=} \int_0^\infty \mathbb{E}_{I^{\text{sens}}} \left[e^{-\frac{r^{\alpha_R} T^{\text{sens}} (I^{\text{sens}} + N^{\text{sens}})}{\sigma_{\text{rcs}} k_R}} \right] f_{\tilde{R}_0}(r) dr \\
 & \stackrel{(b)}{=} \int_0^\infty e^{-\frac{r^{\alpha_R} T^{\text{sens}} N^{\text{sens}}}{\sigma_{\text{rcs}} k_R}} \mathcal{L}_{I^{\text{sens}}} \left(\frac{r^{\alpha_R} T^{\text{sens}}}{\sigma_{\text{rcs}} k_R} \right) f_{\tilde{R}_0}(r) dr,
 \end{aligned} \tag{54}$$

where (a) follows from the CCDF of the RCS in Eq. (18), (b) follows from the definition of Laplace transform. With

the considered interference model in Eq. (11), the Laplace function of I^{sens} then can be expressed as

$$\begin{aligned}
 \mathcal{L}_{I^{\text{sens}}}(s) & = \int_0^\infty e^{-sI^{\text{sens}}} f(I^{\text{sens}}) dI^{\text{sens}} \\
 & = \mathbb{E} \left[e^{-sI^{\text{sens}}} \right] \\
 & = \mathbb{E} \left[e^{-s(I_{\text{LoS}}^{\text{sens}} + I_{\text{NLoS}}^{\text{sens}} + I_{\text{TRC}}^{\text{sens}})} \right] \\
 & = \mathcal{L}_{I_{\text{LoS}}^{\text{sens}}}(s) \mathcal{L}_{I_{\text{NLoS}}^{\text{sens}}}(s) \mathcal{L}_{I_{\text{TRC}}^{\text{sens}}}(s).
 \end{aligned} \tag{55}$$

Since the random variables $g_{L,i}^{\text{sens}}$, \hat{S}_i and the point process Φ_{bs} are independent of each other, similar to the proof process for Theorem 1, we have

$$\begin{aligned}
 \mathcal{L}_{I_{\text{LoS}}^{\text{sens}}}(s) & \\
 & = \mathbb{E}_{\Phi_{\text{bs}}, \{g_{L,i}^{\text{sens}}\}, \{\hat{S}_i\}} \left[e^{-s \sum_{i \in \Phi_{\text{bs}}} g_{L,i}^{\text{sens}} \text{PL}_L(\hat{R}_i) \hat{S}_i} \right] \\
 & = \mathbb{E}_{\Phi_{\text{bs}}, \{g_{L,i}^{\text{sens}}\}, \{\hat{S}_i\}} \left[\prod_{i \in \Phi_{\text{bs}}} e^{-sg_{L,i}^{\text{sens}} k_L \hat{R}_i^{-\alpha_L} \hat{S}_i} \right] \\
 & \stackrel{(c)}{=} \mathbb{E}_{\Phi_{\text{bs}}} \left[\prod_{i \in \Phi_{\text{bs}}} \left[\mathbb{E}_{\{g_{L,i}^{\text{sens}}\}} \left[e^{-sg_{L,i}^{\text{sens}} k_L \hat{R}_i^{-\alpha_L}} \right] \right. \right. \\
 & \quad \left. \left. \times \text{Pr}_L(\hat{R}_i) + \text{Pr}_N(\hat{R}_i) \right] \right],
 \end{aligned} \tag{56}$$

where (c) uses $\hat{S}_i \sim \text{Bernoulli}(\text{Pr}_L(\hat{R}_i))$. The small-scale fading of the LoS path is modeled as Rician fading, so the expectation in Eq. (56) with respect to $g_{L,i}^{\text{sens}}$ can be computed as

$$\begin{aligned}
 \mathbb{E}_{\{g_{L,i}^{\text{sens}}\}} \left[e^{-sg_{L,i}^{\text{sens}} k_L \hat{R}_i^{-\alpha_L}} \right] & \\
 & = \int_0^\infty e^{-sxk_L \hat{R}_i^{-\alpha_L}} f_{g_{L,i}^{\text{sens}}}(x) dx \\
 & \stackrel{(d)}{\approx} \sum_{n=0}^N w_n^K \int_0^\infty u_n^K e^{-sxk_L \hat{R}_i^{-\alpha_L}} e^{-u_n^K x} dx \\
 & = \sum_{n=1}^N w_n^K \frac{u_n^K}{u_n^K + sk_L \hat{R}_i^{-\alpha_L}},
 \end{aligned} \tag{57}$$

where (d) is obtained using the approximate PDF of $g_{L,i}^{\text{sens}}$ in Eq. (13). Substituting Eq. (57) into Eq. (56) yields that

$$\begin{aligned}
 \mathcal{L}_{I_{\text{LoS}}^{\text{sens}}}(s) & \\
 & \approx \mathbb{E}_{\Phi_{\text{bs}}} \left[\prod_{i \in \Phi_{\text{bs}}} \left[\sum_{n=1}^N w_n^K \frac{u_n^K \text{Pr}_L(\hat{R}_i)}{u_n^K + sk_L \hat{R}_i^{-\alpha_L}} + \text{Pr}_N(\hat{R}_i) \right] \right] \\
 & \stackrel{(e)}{=} \exp \left[-2\pi \lambda_{\text{bs}} \int_r^\infty x \left[1 - \sum_{n=1}^N w_n^K \frac{u_n^K \text{Pr}_L(x)}{u_n^K + sk_L x^{-\alpha_L}} \right. \right. \\
 & \quad \left. \left. - \text{Pr}_N(x) \right] dx \right] \\
 & = \exp \left[-2\pi \lambda_{\text{bs}} \sum_{n=1}^N w_n^K \int_r^\infty x \left(\frac{sk_L \text{Pr}_L(x)}{u_n^K x^{\alpha_L} + sk_L} \right) dx \right] \\
 & = \exp \left[-2\pi \lambda_{\text{bs}} \sum_{n=1}^N w_n^K \mathbb{F} \left(\frac{u_n^K}{sk_L}, \alpha_L, \text{Pr}_L(x), r \right) \right],
 \end{aligned} \tag{58}$$

where (e) uses the PGFL of PPP, $\mathbb{F}(\varepsilon, \alpha, p(x), h) = \int_h^\infty \frac{xp(x)}{\varepsilon x^\alpha + 1} dx$. Note that when using PGFL, the lower bound of the integral starts at r rather than at 0. This is because sensing is associated with the nearest visible BS, and no other visible BS will exist within a circle with radius r and center ST. This fraction needs to be shaved from the plane when calculating LoS interference.

Similarly, Laplace transform of NLoS interference links can be derived as

$$\begin{aligned} \mathcal{L}_{\text{NLoS}}^{\text{sens}}(s) &= \mathbb{E}_{\Phi_{\text{bs}}, \{g_{N,i}^{\text{sens}}\}, \{\hat{S}_i\}} \left[e^{-s \sum_{i \in \Phi_{\text{bs}}} g_{N,i}^{\text{sens}} \text{Pr}_L(\hat{R}_i)(1-\hat{S}_i)} \right] \\ &= \mathbb{E}_{\Phi_{\text{bs}}, \{g_{N,i}^{\text{sens}}\}, \{\hat{S}_i\}} \left[\prod_{i \in \Phi_{\text{bs}}} e^{-s g_{N,i}^{\text{sens}} k_N \hat{R}_i^{-\alpha_N} (1-\hat{S}_i)} \right] \\ &\stackrel{(f)}{=} \mathbb{E}_{\Phi_{\text{bs}}} \left[\prod_{i \in \Phi_{\text{bs}}} \left[\mathbb{E}_{\{g_{N,i}^{\text{sens}}\}} \left[e^{-s g_{N,i}^{\text{sens}} k_N \hat{R}_i^{-\alpha_N}} \right] \right. \right. \\ &\quad \left. \left. \times \text{Pr}_N(\hat{R}_i) + \text{Pr}_L(\hat{R}_i) \right] \right], \end{aligned} \quad (59)$$

where (f) holds because $\hat{S}_i \sim \text{Bernoulli}(\text{Pr}_L(\hat{R}_i))$, and $g_{N,i}^{\text{sens}}$, \hat{S}_i and the point process Φ_{bs} are independent of each other. The expectation with respect to $g_{N,i}^{\text{sens}}$ can be formulated as follows

$$\begin{aligned} \mathbb{E}_{\{g_{N,i}^{\text{sens}}\}} \left[e^{-s g_{N,i}^{\text{sens}} k_N R_i^{-\alpha_N}} \right] &= \int_0^\infty e^{-s x k_N R_i^{-\alpha_N}} f_{g_{N,i}^{\text{sens}}}(x) dx \\ &\stackrel{(g)}{=} \mu_N^{\text{sens}} \int_0^\infty e^{-x(\mu_N^{\text{sens}} + s k_N R_i^{-\alpha_N})} dx \\ &= \frac{\mu_N^{\text{sens}}}{\mu_N^{\text{sens}} + s k_N R_i^{-\alpha_N}}, \end{aligned} \quad (60)$$

where (g) holds because the the PDF of $g_{N,i}^{\text{sens}}$ in Eq. (15). Hence,

$$\begin{aligned} \mathcal{L}_{\text{NLoS}}^{\text{sens}}(s) &= \mathbb{E}_{\Phi_{\text{bs}}} \left[\prod_{i \in \Phi_{\text{bs}}} \left[\frac{\mu_N^{\text{sens}} \text{Pr}_N(\hat{R}_i)}{\mu_N^{\text{sens}} + s k_N \hat{R}_i^{-\alpha_N}} + \text{Pr}_L(\hat{R}_i) \right] \right] \\ &\stackrel{(h)}{=} \exp \left[-2\pi \lambda_{\text{bs}} \int_0^\infty x \left(\frac{s k_N \text{Pr}_N(x)}{\mu_N^{\text{sens}} x^{\alpha_N} + s k_N} \right) dx \right] \\ &= \exp \left[-2\pi \lambda_{\text{bs}} \mathbb{F} \left(\frac{\mu_N^{\text{sens}}}{s k_N}, \alpha_N, \text{Pr}_N(x), 0 \right) \right], \end{aligned} \quad (61)$$

where (h) uses the PGFL. The integration starts from 0 because the association policy is only relevant for BSs where LoS is present and does not affect NLoS BSs.

In the same vein,

$$\begin{aligned} \mathcal{L}_{\text{TRC}}^{\text{sens}}(s) &= \mathbb{E}_{\Phi_{\text{bs}}, \sigma_{\text{rcs}}, \{\tilde{S}_i\}} \left[e^{-s \sum_{i \in \Phi_{\text{bs}}} \sigma_{\text{rcs}} k_R \tilde{R}_i^{-\alpha_L} \tilde{S}_i \times \tilde{R}_0^{-\alpha_L} \tilde{S}_0} \right] \\ &= \mathbb{E}_{\Phi_{\text{bs}}, \sigma_{\text{rcs}}, \{\tilde{S}_i\}} \left[\prod_{i \in \Phi_{\text{bs}}} e^{-s \sigma_{\text{rcs}} k_R \tilde{R}_i^{-\alpha_L} \tilde{S}_i \times \tilde{R}_0^{-\alpha_L} \tilde{S}_0} \right] \\ &\stackrel{(i)}{=} \mathbb{E}_{\Phi_{\text{bs}}} \left[\prod_{i \in \Phi_{\text{bs}}} \left[\mathbb{E}_{\sigma_{\text{rcs}}} \left[e^{-s k_R \sigma_{\text{rcs}} \tilde{R}_i^{-\alpha_L} \tilde{R}_0^{-\alpha_L}} \right] \text{Pr}_L(\tilde{R}_i) \right. \right. \\ &\quad \left. \left. + \text{Pr}_N(\tilde{R}_i) \right] \right] \\ &\stackrel{(j)}{=} \mathbb{E}_{\Phi_{\text{bs}}} \left[\prod_{i \in \Phi_{\text{bs}}} \left[\frac{\text{Pr}_L(\tilde{R}_i)}{1 + s k_R \bar{\sigma}_{\text{rcs}} \tilde{R}_i^{-\alpha_L} \tilde{R}_0^{-\alpha_L}} + \text{Pr}_N(\tilde{R}_i) \right] \right] \\ &\stackrel{(k)}{=} \exp \left[-2\pi \lambda_{\text{bs}} \int_r^\infty x \left(\frac{s k_R \text{Pr}_L(x)}{\bar{\sigma}_{\text{rcs}}^{-1} x^{\alpha_L} r^{\alpha_L} + s k_R} \right) dx \right] \\ &= \exp \left[-2\pi \lambda_{\text{bs}} \mathbb{F} \left(\frac{r^{\alpha_L}}{s k_R \bar{\sigma}_{\text{rcs}}}, \alpha_L, \text{Pr}_L(x), r \right) \right], \end{aligned} \quad (62)$$

where (i) holds because $\tilde{S}_i \sim \text{Bernoulli}(\text{Pr}_L(\tilde{R}_i))$ and $\tilde{S}_0 = 1$, and (j) uses the CCDF of RCS in Eq (18). Since the sensing association strategy is the nearest visible BS, no other visible BS will exist in the circle centered on ST with radius r . Therefore, when PGFL is used in step (k), the integral is calculated from r .

Plugging (58), (61) and (62) into (55) and then into (54) gives the desired result. ■

REFERENCES

- [1] F. Liu, Y. Cui, C. Masouros, J. Xu, T. X. Han, Y. C. Eldar, and S. Buzzi, "Integrated Sensing and Communications: Toward Dual-Functional Wireless Networks for 6G and Beyond," *IEEE J. Sel. Areas Commun.*, vol. 40, no. 6, pp. 1728–1767, Jun. 2022.
- [2] C.-X. Wang, X. You, X. Gao, X. Zhu, Z. Li, C. Zhang, H. Wang, Y. Huang, Y. Chen, H. Haas, J. S. Thompson, E. G. Larsson, M. D. Renzo, W. Tong, P. Zhu, X. Shen, H. V. Poor, and L. Hanzo, "On the Road to 6G: Visions, Requirements, Key Technologies, and Testbeds," *IEEE Commun. Surv. Tutor.*, vol. 25, no. 2, pp. 905–974, Feb. 2023.
- [3] Z. Sun, S. Yan, X. Zhang, and M. Peng, "Modeling and Quantitative Analysis of Motion Detection in CSI-Based Sensing," *IEEE Commun. Lett.*, vol. 26, no. 11, pp. 2809–2813, Nov. 2022.
- [4] Y. Huang, J. Yang, W. Tang, C.-K. Wen, S. Xia, and S. Jin, "Joint Localization and Environment Sensing by Harnessing NLOS Components in RIS-Aided mmWave Communication Systems," *IEEE Trans. Wirel. Commun.*, vol. 22, no. 12, pp. 8797–8813, Dec. 2023.
- [5] X. Tong, Z. Zhang, Y. Zhang, Z. Yang, C. Huang, K.-K. Wong, and M. Debbah, "Environment Sensing Considering the Occlusion Effect: A Multi-View Approach," *IEEE Trans. Signal Process.*, vol. 70, pp. 3598–3615, Jun. 2022.
- [6] F. Liu, C. Masouros, A. P. Petropulu, H. Griffiths, and L. Hanzo, "Joint Radar and Communication Design: Applications, State-of-the-Art, and the Road Ahead," *IEEE Trans. Commun.*, vol. 68, no. 6, pp. 3834–3862, Jun. 2020.
- [7] Y. Cui, F. Liu, X. Jing, and J. Mu, "Integrating Sensing and Communications for Ubiquitous IoT: Applications, Trends, and Challenges," *IEEE Netw.*, vol. 35, no. 5, pp. 158–167, Sep. 2021.
- [8] X. Liu, T. Huang, N. Shlezinger, Y. Liu, J. Zhou, and Y. C. Eldar, "Joint Transmit Beamforming for Multiuser MIMO Communications and MIMO Radar," *IEEE Trans. Signal Process.*, vol. 68, pp. 3929–3944, Jun. 2020.
- [9] Y. Zhong, T. Bi, J. Wang, J. Zeng, Y. Huang, T. Jiang, Q. Wu, and S. Wu, "Empowering the V2X Network by Integrated Sensing and Communications: Background, Design, Advances, and Opportunities," *IEEE Netw.*, vol. 36, no. 4, pp. 54–60, Jul. 2022.

- [10] D. Wu, Y. Zeng, R. Gao, S. Li, Y. Li, R. C. Shah, H. Lu, and D. Zhang, "WiTraj: Robust Indoor Motion Tracking With WiFi Signals," *IEEE Trans. Mob. Comput.*, vol. 22, no. 5, pp. 3062–3078, May 2023.
- [11] X. Li, J. He, Z. Yu, G. Wang, and P. Zhu, "Integrated Sensing and Communication in 6G: The Deterministic Channel Models for THz Imaging," in *2021 IEEE 32nd Annual International Symposium on Personal, Indoor and Mobile Radio Communications (PIMRC)*, Sep. 2021, pp. 1–6.
- [12] Y. Ma, Z. Yuan, S. Xia, G. Yu, and L. Hu, "Highly Efficient Waveform Design and Hybrid Duplex for Joint Communication and Sensing," *IEEE Internet Things J.*, vol. 10, no. 19, pp. 17 369–17 381, Oct. 2023.
- [13] 3GPP, "Study on Integrated Sensing and Communication," 3rd Generation Partnership Project (3GPP), Sophia Antipolis, France, Technical Specification (TS) 22.837, Mar. 2022.
- [14] J. A. Zhang, M. L. Rahman, K. Wu, X. Huang, Y. J. Guo, S. Chen, and J. Yuan, "Enabling Joint Communication and Radar Sensing in Mobile Networks—A Survey," *IEEE Commun. Surv. Tutor.*, vol. 24, no. 1, pp. 306–345, Oct. 2021.
- [15] L. Zheng, M. Lops, Y. C. Eldar, and X. Wang, "Radar and Communication Coexistence: An Overview: A Review of Recent Methods," *IEEE Signal Process. Mag.*, vol. 36, no. 5, pp. 85–99, Sep. 2019.
- [16] A. R. Chiriyath, B. Paul, and D. W. Bliss, "Radar-Communications Convergence: Coexistence, Cooperation, and Co-Design," *IEEE Trans. Cogn. Commun. Netw.*, vol. 3, no. 1, pp. 1–12, Mar. 2017.
- [17] C. Dou, N. Huang, Y. Wu, L. Qian, and T. Q. S. Quek, "Channel Sharing aided Integrated Sensing and Communication: An Energy-Efficient Sensing Scheduling Approach," *IEEE Trans. Wirel. Commun.*, pp. 1–15, Oct. 2023.
- [18] G. Wu, Y. Fang, J. Xu, Z. Feng, and S. Cui, "Energy-Efficient MIMO Integrated Sensing and Communications With On-off Non-Transmission Power," *IEEE Internet Things J.*, pp. 1–16, Nov. 2023.
- [19] J. A. Zhang, F. Liu, C. Masouros, R. W. Heath, Z. Feng, L. Zheng, and A. Petropulu, "An Overview of Signal Processing Techniques for Joint Communication and Radar Sensing," *IEEE J. Sel. Top. Signal Process.*, vol. 15, no. 6, pp. 1295–1315, Nov. 2021.
- [20] A. Liu, Z. Huang, M. Li, Y. Wan, W. Li, T. X. Han, C. Liu, R. Du, D. K. P. Tan, J. Lu, Y. Shen, F. Colone, and K. Chetty, "A Survey on Fundamental Limits of Integrated Sensing and Communication," *IEEE Commun. Surv. Tutor.*, vol. 24, no. 2, pp. 994–1034, Feb. 2022.
- [21] C. Li, N. Raymondi, B. Xia, and A. Sabharwal, "Outer Bounds for a Joint Communicating Radar (Comm-Radar): The Uplink Case," *IEEE Trans. Commun.*, vol. 70, no. 2, pp. 1197–1213, Nov. 2021.
- [22] C. Ouyang, Y. Liu, and H. Yang, "Performance of Downlink and Uplink Integrated Sensing and Communications (ISAC) Systems," *IEEE Wirel. Commun. Lett.*, vol. 11, no. 9, pp. 1850–1854, Sep. 2022.
- [23] Y. Xiong, F. Liu, Y. Cui, W. Yuan, T. X. Han, and G. Caire, "On the Fundamental Tradeoff of Integrated Sensing and Communications Under Gaussian Channels," *IEEE Trans. Inf. Theory*, vol. 69, no. 9, pp. 5723–5751, Sep. 2023.
- [24] Z. Xiao and Y. Zeng, "Waveform Design and Performance Analysis for Full-Duplex Integrated Sensing and Communication," *IEEE J. Sel. Areas Commun.*, vol. 40, no. 6, pp. 1823–1837, Jun. 2022.
- [25] X. Cheng, D. Duan, S. Gao, and L. Yang, "Integrated Sensing and Communications (ISAC) for Vehicular Communication Networks (VCN)," *IEEE Internet Things J.*, vol. 9, no. 23, pp. 23 441–23 451, Dec. 2022.
- [26] K. Meng, C. Masouros, G. Chen, and F. Liu, "Network-Level Integrated Sensing and Communication: Interference Management and BS Coordination Using Stochastic Geometry," *arXiv:2311.09052v1 [cs.IT]*, Nov. 2023.
- [27] Z. Wei, F. Liu, C. Masouros, N. Su, and A. P. Petropulu, "Toward Multi-Functional 6G Wireless Networks: Integrating Sensing, Communication, and Security," *IEEE Commun. Mag.*, vol. 60, no. 4, pp. 65–71, Apr. 2022.
- [28] X. Liu, H. Zhang, K. Long, A. Nallanathan, and V. C. M. Leung, "Distributed Unsupervised Learning for Interference Management in Integrated Sensing and Communication Systems," *IEEE Trans. Wirel. Commun.*, vol. 22, no. 12, pp. 9301–9312, Dec. 2023.
- [29] Y. Hmamouche, M. Benjillali, S. Saoudi, H. Yanikomeroglu, and M. D. Renzo, "New Trends in Stochastic Geometry for Wireless Networks: A Tutorial and Survey," *Proc. IEEE*, vol. 109, no. 7, pp. 1200–1252, Jul. 2021.
- [30] X. Zhang, M. Peng, and C. Liu, "Impacts of Antenna Downtilt and Backhaul Connectivity on the UAV-Enabled Heterogeneous Networks," *IEEE Trans. Wirel. Commun.*, vol. 22, no. 6, pp. 4057–4073, Jun. 2023.
- [31] N. Okati, T. Riihonen, D. Korpi, I. Angervuori, and R. Wichman, "Downlink Coverage and Rate Analysis of Low Earth Orbit Satellite Constellations Using Stochastic Geometry," *IEEE Trans. Commun.*, vol. 68, no. 8, pp. 5120–5134, Aug. 2020.
- [32] P. Ren, A. Munari, and M. Petrova, "Performance Tradeoffs of Joint Radar-Communication Networks," *IEEE Wirel. Commun. Lett.*, vol. 8, no. 1, pp. 165–168, Feb. 2019.
- [33] N. R. Olson, J. G. Andrews, and R. W. Heath Jr, "Coverage and Capacity of Joint Communication and Sensing in Wireless Networks," *arXiv:2210.02289v1 [cs.IT]*, Oct. 2022.
- [34] C. Skouroumounis, C. Psomas, and I. Krikidis, "FD-JCAS Techniques for mmWave HetNets: Ginibre Point Process Modeling and Analysis," *IEEE Trans. Mob. Comput.*, vol. 21, no. 12, pp. 4352–4366, Dec. 2022.
- [35] H. Ma, Z. Wei, Z. Li, F. Ning, X. Chen, and Z. Feng, "Performance of Cooperative Detection in Joint Communication-Sensing Vehicular Network: A Data Analytic and Stochastic Geometry Approach," *IEEE Trans. Veh. Technol.*, vol. 72, no. 3, pp. 3848–3863, Mar. 2023.
- [36] T. Bai, R. Vaze, and R. W. Heath, "Analysis of Blockage Effects on Urban Cellular Networks," *IEEE Trans. Wirel. Commun.*, vol. 13, no. 9, pp. 5070–5083, Sep. 2014.
- [37] 3GPP, "Study on channel model for frequencies from 0.5 to 100 GHz," 3rd Generation Partnership Project (3GPP), Technical Specification (TS) 38.901 Version 16.1.0 Release 16, Nov. 2020.
- [38] J. G. Andrews, F. Baccelli, and R. K. Ganti, "A Tractable Approach to Coverage and Rate in Cellular Networks," *IEEE Trans. Commun.*, vol. 59, no. 11, pp. 3122–3134, Nov. 2011.
- [39] S. Yan, M. Peng, and X. Cao, "A Game Theory Approach for Joint Access Selection and Resource Allocation in UAV Assisted IoT Communication Networks," *IEEE Internet Things J.*, vol. 6, no. 2, pp. 1663–1674, Apr. 2019.
- [40] X. Yang and A. O. Fapojuwo, "Coverage Probability Analysis of Heterogeneous Cellular Networks in Rician/Rayleigh Fading Environments," *IEEE Commun. Lett.*, vol. 19, no. 7, pp. 1197–1200, Jul. 2015.
- [41] P. Swerling, "Probability of detection for fluctuating targets," *IRE Trans. Inf. Theory*, vol. 6, no. 2, pp. 269–308, Apr. 1960.
- [42] M. I. Skolnik, *Introduction to Radar Systems*, 3rd ed. New York, NY, USA: McGraw-Hill, Dec. 2002.



Zezhong Sun (Student Member, IEEE) received the B.S. degree in information engineering from Beijing University of Posts and Telecommunications (BUPT), Beijing, China, in 2019. He is currently working toward the Ph.D. degree in Information and Communication Engineering at the State Key Laboratory of Networking and Switching Technology (SKT-NST), BUPT. His research interests include information theory on integrated sensing and communications (ISAC), stochastic geometry and wireless sensing.



Shi Yan (Member, IEEE) received the Ph.D. degree in communication and information engineering from Beijing University of Posts and Telecommunications (BUPT), Beijing, China, in 2017. He is currently an Associate Professor with the State Key Laboratory of Networking and Switching Technology (SKT-NST), BUPT. In 2015, he was an Academic Visiting Scholar with Arizona State University, Tempe, AZ, USA. His research interests include game theory, integrated sensing and communication (ISAC), resource management, deep reinforcement learning, stochastic geometry, and fog radio access networks.



Ning Jiang (Student Member, IEEE) received the B.S. degree and M.S. degree in information and communication engineering from the Beijing University of Posts and Telecommunications (BUPT), Beijing, China, in 2020 and 2023, where he is currently pursuing the Ph.D degree with the State Key Laboratory of Networking and Switching Technology (SKT-NST), BUPT. His current research interests include integrated sensing and communication (ISAC), resource management, performance analysis and machine learning.



Jiaen Zhou (Student Member, IEEE) received the B.S. degree in communication engineering from the Beijing University of Posts and Telecommunications (BUPT), Beijing, China, in 2021, where he is currently pursuing the Ph.D degree with the State Key Laboratory of Networking and Switching Technology (SKT-NST), BUPT. His current research interests include integrated sensing and communication (ISAC), resource management and space-air-ground integrated networks.



Mugen Peng (Fellow, IEEE) received the Ph.D. degree in communication and information systems from the Beijing University of Posts and Telecommunications (BUPT), Beijing, China, in 2005. Afterward, he joined BUPT, where he has been a Full Professor with the School of Information and Communication Engineering since 2012. During 2014 he was also an academic visiting fellow at Princeton University, NJ, USA. He leads a Research Group focusing on wireless transmission and networking technologies in BUPT. He has authored and coauthored over 100 refereed IEEE journal papers and over 300 conference proceeding papers. His main research areas include wireless communication theory, radio signal processing, cooperative communication, self-organization networking, heterogeneous networking, cloud communication, and Internet of Things. Prof. Peng was a recipient of the 2018 Heinrich Hertz Prize Paper Award; the 2014 IEEE ComSoc AP Outstanding Young Researcher Award; and the Best Paper Award in the ICC 2022, JCN 2016, IEEE WCNC 2015, IEEE GameNets 2014, IEEE CIT 2014, ICCTA 2011, IC-BNMT 2010, and IET CCWMC 2009. He is on the Editorial/Associate Editorial Board of the IEEE Communications Magazine, IEEE Access, the IEEE Internet of Things Journal, IET Communications, and China Communications. He is the Fellow of IEEE and IET.